First Principle Exploration of (K, Rb)(Al, Si)O_3 Perovskites: Structural, Elastic, Anisotropic, Electronic, and Lattice Dynamical Properties

Ü. Bayhan[a] and İ. Yilmaz[b,*]

[a] *Department of Physics, Burdur Mehmet Akif Ersoy University, Istiklal Campus, 15030, Burdur, Turkey*
[b] *Department of Physics, Burdur Mehmet Akif Ersoy University, Graduate School of Natural and Applied Sciences, Istiklal Campus, Burdur 15030, Turkey*

Received: 13.03.2023 & Accepted: 26.06.2023

Doi: 10.12693/APhysPolA.144.99 *e-mail: inanc91@gmail.com

This study explained the structural, elastic, anisotropic, electronic, and lattice dynamical properties of (K, Rb)(Al, Si)O_3, using both the generalized gradient and local density approximations with *density functional theory* implemented by the Vienna *Ab Initio* Simulation Package. The calculated elastic constants revealed that current compounds are mechanically stable; over and above, the bulk and shear moduli, Young's modulus, and Poisson's ratio of the compounds investigated were derived from the calculated elastic constants of the compounds considered. Additionally, the electronic behavior of (K, Rb)(Al, Si)O_3 compounds has been explored. The work discovered that the current compounds demonstrated half-metallicity properties relatedly to their electronic properties. The charge transportation of the compounds considered has been assessed utilizing *Bader* charge analysis. Furthermore, the compounds investigated have demonstrated a dominantly ionic bonding nature. Besides, except for $KSiO_3$, the calculated magnetic moment was determined to be around 2 μ_B for $KAlO_3$ and $RbAlO_3$ and 1 μ_B for $RbSiO_3$. The vibrational properties of current compounds were discussed and plotted. It was discovered that the $RbSiO_3$ generalized gradient approximation calculation contains soft modes, although local density approximation has no soft modes. The others are dynamically stable. As far as is known, this study is the first theoretical analysis of (K, Rb)SiO_3 perovskites, and experimental confirmations are still pending. This article can assist in better understanding the compounds considered and motivate further studies.

topics: cubic perovskites, phonons, half-metallicity, electronic properties

1. Introduction

Perovskite structures exhibit a variety of peculiar features and are desirable in various types of applications for this reason. A number of studies on these compounds have been reported in numerous fields. Some of these reports are related to as follows: high stabilization in solar cell applications [1–5], magnetism, ferroelectricity, and superconductivity [6–14], half-metallicity [15], hydrogen sensors and capability of solid-state hydrogen storage [16, 17].

In this essay, the structural, elastic, anisotropic elastic, electronic, lattice dynamical, and thermodynamical properties of $KAlO_3$, $RbAlO_3$, $KSiO_3$, and $RbSiO_3$ for both types of calculation are investigated. This article seeks to demonstrate that these discussed properties have a pivotal role as far as potential areas related to the use of the compound are concerned. This essay is organized as follows. Sect. 2 describes the calculating process. The results in Sect. 3 include structural properties in Sect. 3.1, mechanical properties in Sect. 3.2, anisotropic properties in Sect. 3.3, electronic properties in Sect. 3.4, and lattice dynamical and thermodynamic properties in Sect. 3.5. Finally, Sect. 4 concludes the study. In addition, other outcomes related to mechanical qualities are presented in Appendix A. Also, anisotropic properties are reported in Appendix B.

2. Calculation details

The density functional theory (DFT) calculations have been performed using the Vienna *Ab Initio* Simulation Package (VASP) [18, 19]. VASP with projector augmented wave (PAW) [20, 21] pseudopotentials with 600 eV cut-off energy based on DFT were used to study total energy and linked characteristics of (K, Rb)(Al, Si)O_3 perovskites in detail. The Perdew–Burke–Ernzerhof functional (PBE) with generalized gradient approximation (GGA) [22] was utilized to stand for the exchange–correlation terms in electron–electron interactions.

On the other hand, the Perdew–Zunger (PZ) parametrization of the Ceperley–Alder (CA) Monte Carlo correlation functional was used to represent the exchange–correlation terms in electron–electroninteractions in the local density approximation (LDA) [23–25]. The calculations for compounds considered have been executed with a gamma-centered $24 \times 24 \times 24$ $k-$ points [26] scheme with an automatic mesh. Furthermore, the smearing was set to 0.125 eV using the Methfessel–Paxton (MP) scheme [27]. The convergence points, such as EDIFF and EDIFFG tags in VASP, have been agreed to be at 10^{-10} eV and 10^{-8} eV Å^{-1}, respectively. The ISIF parameter in VASP was adjusted to 3 to relax cell volume and ion environments in (K, Rb)(Al, Si)O_3 perovskites. Following that, the optimal structural parameters acquired were used in each computation for each compound. Moreover, the Visualization for Electronic and STructural Analysis (VESTA) program [28] was used to visualize the optimized geometry. The stress–strain [18, 19, 29] approach was used to compute the elastic constants for the compounds considered. The anisotropic properties obtained from the calculated elastic constants were computed and visualized using Elastic tensor analysis (ELATE) [30], an open-source online tool structured from the Elastic Anisotropy Measures (EIAM) code [31]. Using the Phonopy code [32], which is based on density-functional perturbation theory (DFPT) [33], the linear response technique was utilized to investigate the lattice dynamical properties of (K, Rb)(Al, Si)O_3 perovskites. The present compounds' phonon dispersion curves and density of states were plotted using Phonopy, which expanded the unit cell by $2 \times 2 \times 2$. Thermal properties were also assessed for each compound under consideration.

3. Results

3.1. Structural properties

The perovskite oxides generally crystallize in cubic symmetry in the $Pm\bar{3}m$ (#221) space group. Accordingly, these atoms can take the following Wyckoff positions: 1a (0.0, 0.0, 0.0) for the K, Rb atoms; 1b (0.5, 0.5, 0.5) for the Al, Si atoms; and 3c (0.0, 0.5, 0.5), (0.5, 0.0, 0.5), (0.5, 0.5, 0.0) for the last O atoms. Figure 1 demonstrates the crystal structure of perovskite oxides under investigation.

Figure 2 illustrates the energy–volume relationship of the compounds under examination in the ferromagnetic (FM) and anti-ferromagnetic (AFM) phases for GGA and LDA. As demonstrated in Fig. 2, the GGA calculation of $KAlO_3$ has an AFM phase, but the one of LDA has an FM state. Since LDA is comprehended to overbind and GGA is understood to smoothen interatomic bonds [34–36], these differences are attributed to the chosen approximation. $KSiO_3$ exhibits the same properties.

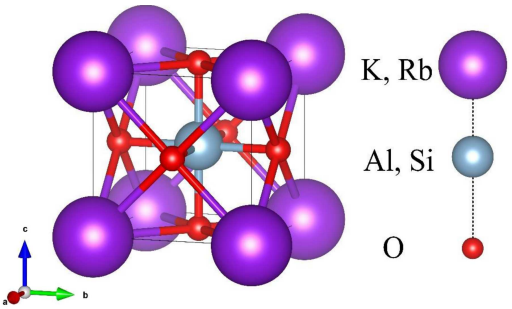

Fig. 1. The crystal structure of (K, Rb)(Al, Si)O_3 compounds.

$RbAlO_3$ and $RbSiO_3$ have FM phases for each calculation type. The lattice constant (a in Å), volume (V in Å^3), density (ρ in g/cm^3), and formation enthalpy (ΔH_f in eV/atom) of (K, Rb)(Al, Si)O_3 perovskites oxides have been cataloged in Table I based on assessment in another study [15]. As shown in Table I, the calculated results are close to those of the other study [15]. These quantities presented play quite a pivotal role in determining the structural properties of compounds. The $KSiO_3$ has the lowest lattice and volume, while $RbAlO_3$ has the highest, considering Table I for both calculation types. Additionally, $RbSiO_3$ has the highest density of the investigated compounds.

The negative formation enthalpy calculated by

$$\Delta H_f = E^{\text{Total}}_{(\text{K, Rb})(\text{Al, Si})\text{O}_3} - \left(E^{\text{Total}}_{(\text{K, Rb})} + E^{\text{Total}}_{(\text{Al, Si})} + 3E^{\text{Total}}_{\text{O}}\right) \quad (1)$$

reveals that the compounds under consideration are both thermodynamically and experimentally stable. The results of the formation enthalpy can demonstrate whether the compound is stable or unstable in terms of thermodynamic stability and synthesis ability. As a result, it is critical in terms of the compound since it contributes to understanding the compound's structure. As can be concluded from the outcomes in Table I, all of the considered compounds are stable, both thermodynamically and experimentally, since they have negative formation enthalpy. Furthermore, according to calculations using either GGA or LDA functionals, $KSiO_3$ is more stable than the other compounds. In the examination using GGA, $RbSiO_3$ has the lowest formation enthalpy; additionally, $RbAlO_3$ has the smallest enthalpy in the computation using LDA.

3.2. Mechanical properties

Mechanical characteristics are pivotal because they hypothetically reveal how compounds respond in technological and portable applications. Therefore, a compound must meet the Born [37] mechanical stability conditions. The stability conditions, which are different for many crystal families,

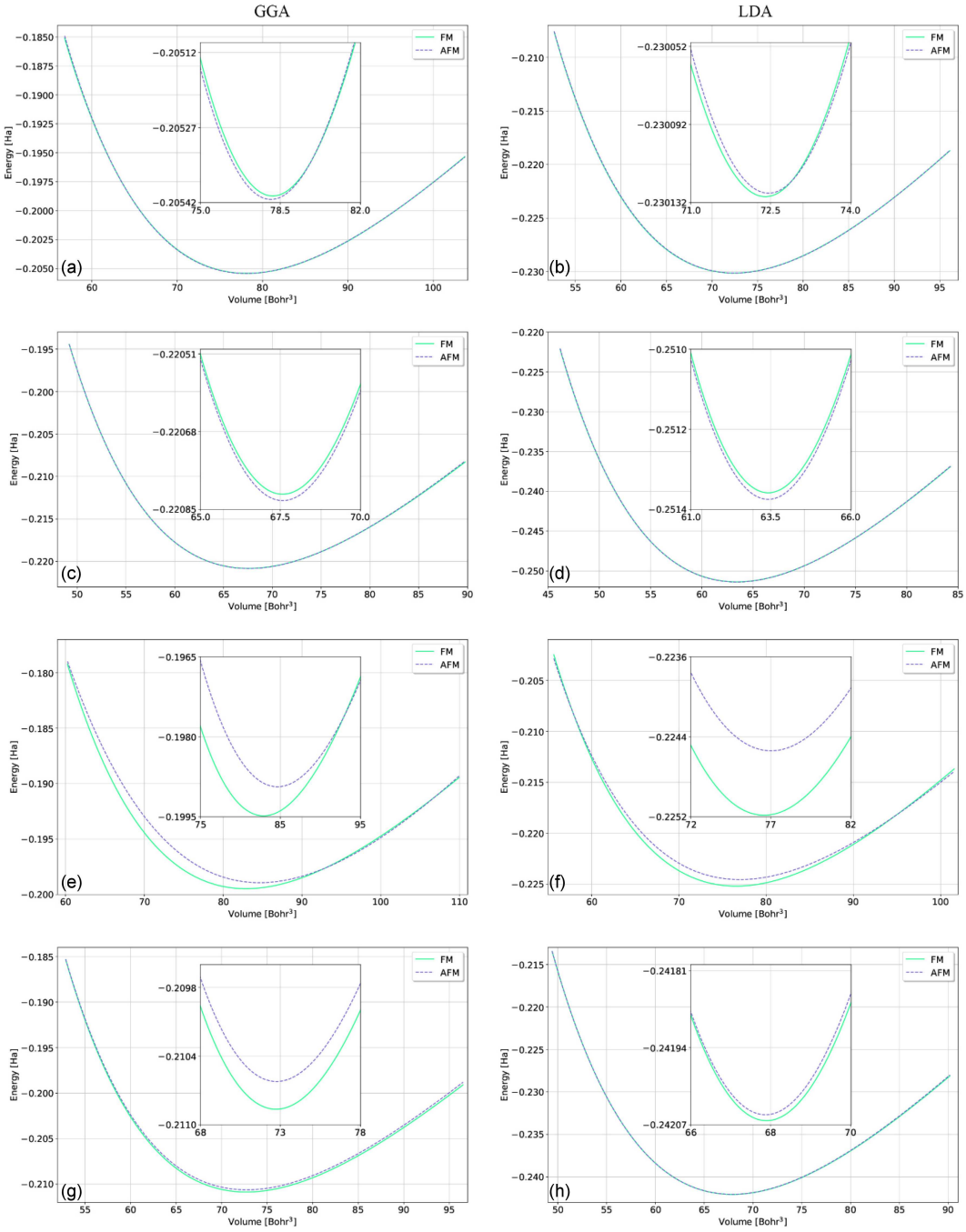

Fig. 2. The Energy [Ha]–volume [Bohr^3] relationship of the (K, Rb)(Al, Si)O_3 compounds (a) $KAlO_3$ GGA (b) $KAlO_3$ LDA (c) $KSiO_3$ GGA (d) $KSiO_3$ LDA (e) $RbAlO_3$ GGA (f) $RbAlO_3$ LDA (g) $RbSiO_3$ GGA (h) $RbSiO_3$ LDA.

are as follows for cubic crystals: $C_{11} - C_{12} > 0$, $C_{11} + 2C_{12} > 0$, $C_{11} > 0$, $C_{44} > 0$. The computed elastic stiffness matrix components, assessed in other investigations [15], have been cataloged in Table II.

As can be concluded from Table II, those compounds under investigation meet the stability conditions. Therefore, it is possible to say that the current compounds are stable as mechanical. The polycrystalline properties obtained from elastic constants and assessed in another study [15] have been mentioned in Table II. The Cauchy pressures (C_p) can be issued to determine if a compound has ductile or brittle behavior. The negative C_p computed exhibits brittleness, whereas the positive one exhibits ductility. As can be deduced from Table II, both the LDA and GGA calculations of $KSiO_3$ have a negative C_p. Therefore, it is possible to explain that $KSiO_3$ exhibits brittle behavior while others demonstrate ductile behavior. Furthermore, $KSiO_3$ has

TABLE I

Lattice parameter (a [Å]), volume (V [Å^3]), density (ρ [g cm^{-3}]), formation enthalpy (ΔH_f [eV/atom]) for (K, Rb)(Al, Si)O_3 perovskites.

Compounds	GGA				LDA			
	a	V	ρ	ΔH_f	a	V	ρ	ΔH_f
$KAlO_3$	3.865	57.714	3.282	−1.663	3.768	53.494	3.541	−2.004
	3.87[a]	–	–	–	–	–	–	–
	3.86[b]	–	–	–	–	–	–	–
$KSiO_3$	3.683	49.959	3.829	−1.750	3.606	46.907	4.078	−2.231
$RbAlO_3$	3.941	61.191	4.354	−1.524	3.838	56.531	4.713	−1.890
	3.95[a]	–	–	–	–	–	–	–
	3.86[b]	–	–	–	–	–	–	–
$RbSiO_3$	3.773	53.717	4.994	−1.501	3.689	50.189	5.345	−1.999

[a]Ferromagnetic (FM), [b]Paramagnetic (PM) results in [15]

TABLE II

The calculated elastic constants (C_{ij} [GPa], Cauchy pressures (C_p [GPa], bulk (B [GPa]), Young (E [GPa]), shear (G [GPa]) moduli, Poisson Ratio (ν), and Vicker's hardness (H_ν [GPa]) polycrystalline properties for (K, Rb)(Al, Si)O_3 perovskites.

Compounds	GGA				LDA			
	$KAlO_3$	$KSiO_3$	$RbAlO_3$	$RbSiO_3$	$KAlO_3$	$KSiO_3$	$RbAlO_3$	$RbSiO_3$
C_{11}	198.513	289.426	162.030	195.647	256.871	359.570	212.886	247.995
C_{12}	78.065	118.803	85.832	135.775	87.149	136.958	99.022	164.082
C_{44}	17.129	146.209	44.772	129.979	27.991	159.285	56.711	150.668
C_p	60.936	−27.406	41.059	5.796	59.158	−22.327	42.311	13.414
B	118.215	175.677	111.231	155.732	143.723	211.162	136.977	192.053
	118.32[a]	–	110.20[a]	–	–	–	–	
	119.62[b]	–	111.74[b]	–	–	–	–	–
E	80.892	288.824	111.848	188.940	120.988	339.898	149.705	234.834
G	29.183	117.792	41.972	72.793	44.491	137.977	56.799	90.585
B/G	4.051	1.491	2.650	2.139	3.230	1.530	2.412	2.120
G/B	0.247	0.671	0.377	0.467	0.310	0.653	0.415	0.472
ν	0.386	0.226	0.332	0.298	0.360	0.232	0.318	0.296
H_ν	2.043	17.091	4.281	8.065	3.562	18.563	5.905	9.513

[a]Ferromagnetic (FM), [b]Paramagnetic (PM) results in [15]

disadvantages for convection-required portable applications due to having negative C_p. Consequently, the other compounds are more suitable than $KSiO_3$ when considering convection-required mobile applications.

The polycrystalline properties can be determined by employing the elastic constants calculated. Bulk (B), Young (E), shear (G) moduli, and Poisson's ratio have been figured out by handling, respectively,

$$B = \frac{B_{\mathrm{V}}}{B_{\mathrm{R}}}, \tag{2}$$

$$E = \frac{9BG}{G+3B}, \tag{3}$$

$$G = \frac{G_{\mathrm{V}}}{G_{\mathrm{R}}}, \tag{4}$$

$$\nu = \frac{1}{2}\frac{B-\frac{2G}{3}}{B+\frac{G}{3}}. \tag{5}$$

Bulk modulus can be handled as an evaluation of the compound's resistance to volume change arising from any applied pressure. Furthermore, the computed B results are near those of the previous studies [15], as shown in Table II. Young's modulus, a gauge of a compound's elasticity, is determined by the stress-to-strain ratio induced by uniaxial deformation. Shear modulus can be assessed as a measure of the compound's strength to elastic shear stiffness, which is calculated by the shear stress to shear strain ratio. Bulk, Young, and shear moduli of (K, Rb)(Al, Si)O_3 perovskites introduced in this work are computed using the Voight [38], Reuss [39], and Hill [40] approximations. Hill approximation, an average of Voigt and Reuss, is in harmony and

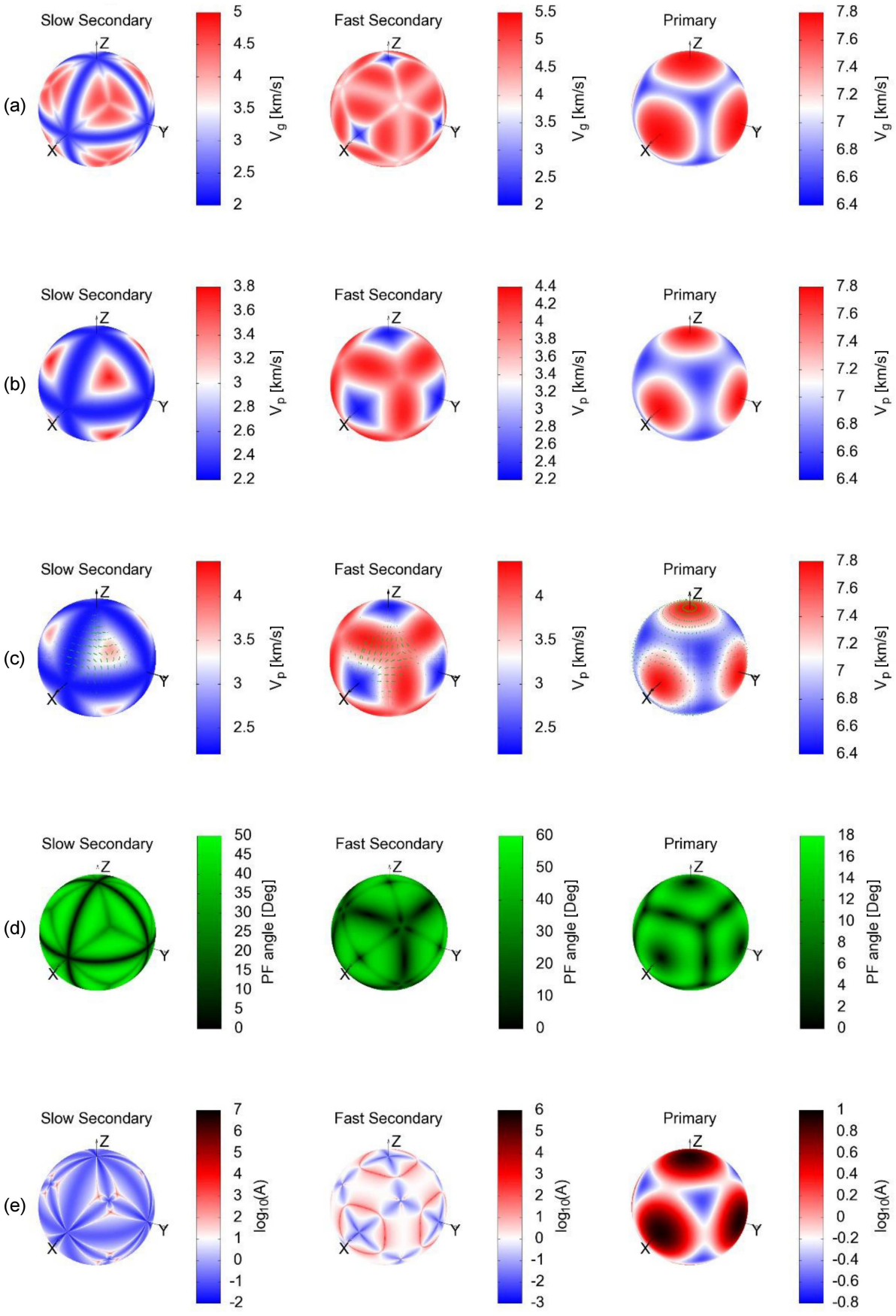

Fig. 3. (a) Group and (b) phase velocities, (c) polarization of sound waves, (d) power flow angles, and (e) enhancement factors for $KAlO_3$ GGA calculation.

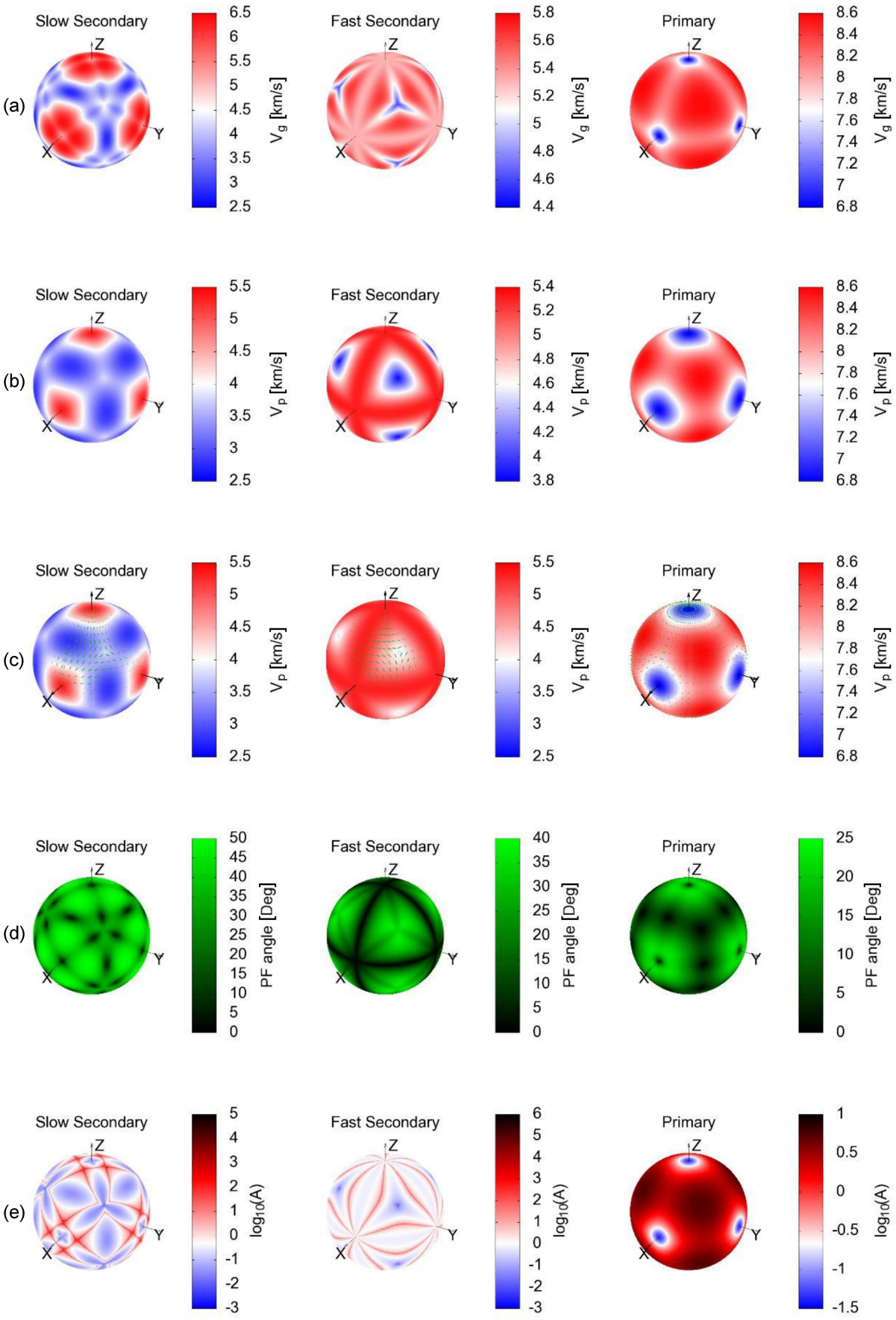

Fig. 4. (a) Group and (b) phase velocities, (c) polarization of sound waves, (d) power flow angles, and (e) enhancement factors for $RbSiO_3$ LDA calculation.

TABLE III

The maximum–minimum points of Young's modulus (E [GPa]), linear compressibility (β [TPa^{-1}]), shear modulus (G [GPa]), and Poisson's ratio (ν) for (K, Rb)(Al, Si)O_3 perovskites.

Compounds	GGA				LDA			
	$KAlO_3$	$KSiO_3$	$RbAlO_3$	$RbSiO_3$	$KAlO_3$	$KSiO_3$	$RbAlO_3$	$RbSiO_3$
$E_{\min}$	49.019	220.280	102.586	84.400	78.856	284.016	149.501	117.326
$E_{\max}$	154.440	343.370	118.426	305.031	212.718	381.837	150.012	358.274
$\beta_{\min}$	2.820	1.897	2.997	2.140	2.319	1.579	2.434	1.736
$\beta_{\max}$	2.820	1.897	2.997	2.140	2.319	1.579	2.434	1.736
$G_{\min}$	17.129	85.312	38.099	29.936	27.991	111.306	56.711	41.957
$G_{\max}$	60.224	146.210	44.772	129.979	84.861	159.285	56.932	150.668
$\nu_{\min}$	0.108	0.030	0.273	-0.290	0.111	0.104	0.317	−0.214
$\nu_{\max}$	0.725	0.398	0.385	0.895	0.672	0.341	0.319	0.803

TABLE IV

Zener anisotropy factor (A), longitudinal wave velocity (V_l [m/s]), transverse wave velocity (V_t [m/s]), mean wave velocity (V_m [m/s]), and Debye temperature ($\theta_{\rm D}$ [K]) for (K, Rb)(Al, Si)O_3 perovskites.

Compounds	GGA				LDA			
	$KAlO_3$	$KSiO_3$	$RbAlO_3$	$RbSiO_3$	$KAlO_3$	$KSiO_3$	$RbAlO_3$	$RbSiO_3$
A	0.284	1.714	1.175	4.342	0.330	1.431	0.996	3.591
V_l	6918.974	9322.738	6196.760	7114.763	7572.264	9844.109	6718.160	7650.434
V_t	2981.829	5546.940	3104.805	3817.904	3990.453	5817.129	3471.594	4116.785
V_t	3368.985	6141.224	3482.587	4263.324	3544.583	6444.530	3886.581	4596.154
$\theta_{\rm D}$	443.817	848.886	449.924	575.231	539.162	909.728	515.548	634.341

more compatible with experimental results. Voigt's approach has been associated with the minimum of these moduli, and Reuss's has been correlated with the maximum. Additionally, the other outcomes can be calculated using bulk and shear modulus. $KSiO_3$ has the highest values for each modulus, while $KAlO_3$ has the lowest ones, taking into account Table II for both computation methods. Similar to Cauchy pressures (C_p), the B/G relation plays a central role in resolving the ductility or brittleness of the compound. Brittleness is indicated by a B/G ratio of less than 1.75; otherwise, ductility is indicated. $KSiO_3$ has a value below the critical rate of B/G for both computation types and exhibits brittle behavior, verifying the conclusions of C_p. Other compounds demonstrate ductile behavior since they have values higher than the critical rate of B/G, agreeing with C_p results again. The G/B ratio — known as Pugh's modulus — is correlated with the bonding characteristics of the compound and plays a central role in introducing the bonding nature. If G/B is approximately 0.6, it means that the compound is the dominantly ionic character, while 1.1 hints at covalent bonding. The investigated compounds have exhibited ionic characteristics due to their G/B being below 0.6, as shown in Table II. The Poisson's ratio, like the G/B ratio, is a significant parameter that is used to determine the compounds' bonding types. If Poisson's ratio is ≈ 0.25, this implies that the compound has a dominantly ionic character, whereas 0.1 indicates covalent bonding. The considered compounds have demonstrated ionic bonding. As argued, these results agree with the G/B outcomes as well.

Another notable criterion in the determination of the rigidity of a compound is Vicker's hardness (H_ν) [41], provided by

$$H_\nu = 0.92k^{1.137}G^{0.708}, \quad \text{with} \quad k = G/B. \tag{6}$$

In addition, H_ν is an exhaustive indicator of the compound's mechanical behavior, propositioned by Tian, depending on bulk and shear modulus. As can be seen in Table II, the H_ν values of these compounds have demonstrated that they are relatively hard compounds due to their H_ν's being below the superhardness restriction [42, 43] ($H_\nu < 40$ GPa).

Figures 3 and 4 demonstrate the group and phase velocities, polarization of sound waves, power flow angles, and enhancement factors of $KAlO_3$ for both calculation types. In the plots, transverse wave velocities are affiliated with the fast and slow secondary modes, whereas longitudinal wave velocities are associated with the primary one. In all axes, transverse wave velocities have a local minimum, while longitudinal wave velocities, except for power flow angles, have a local maximum. It can be seen that the transverse velocities have a local minimum, while longitudinal velocities have

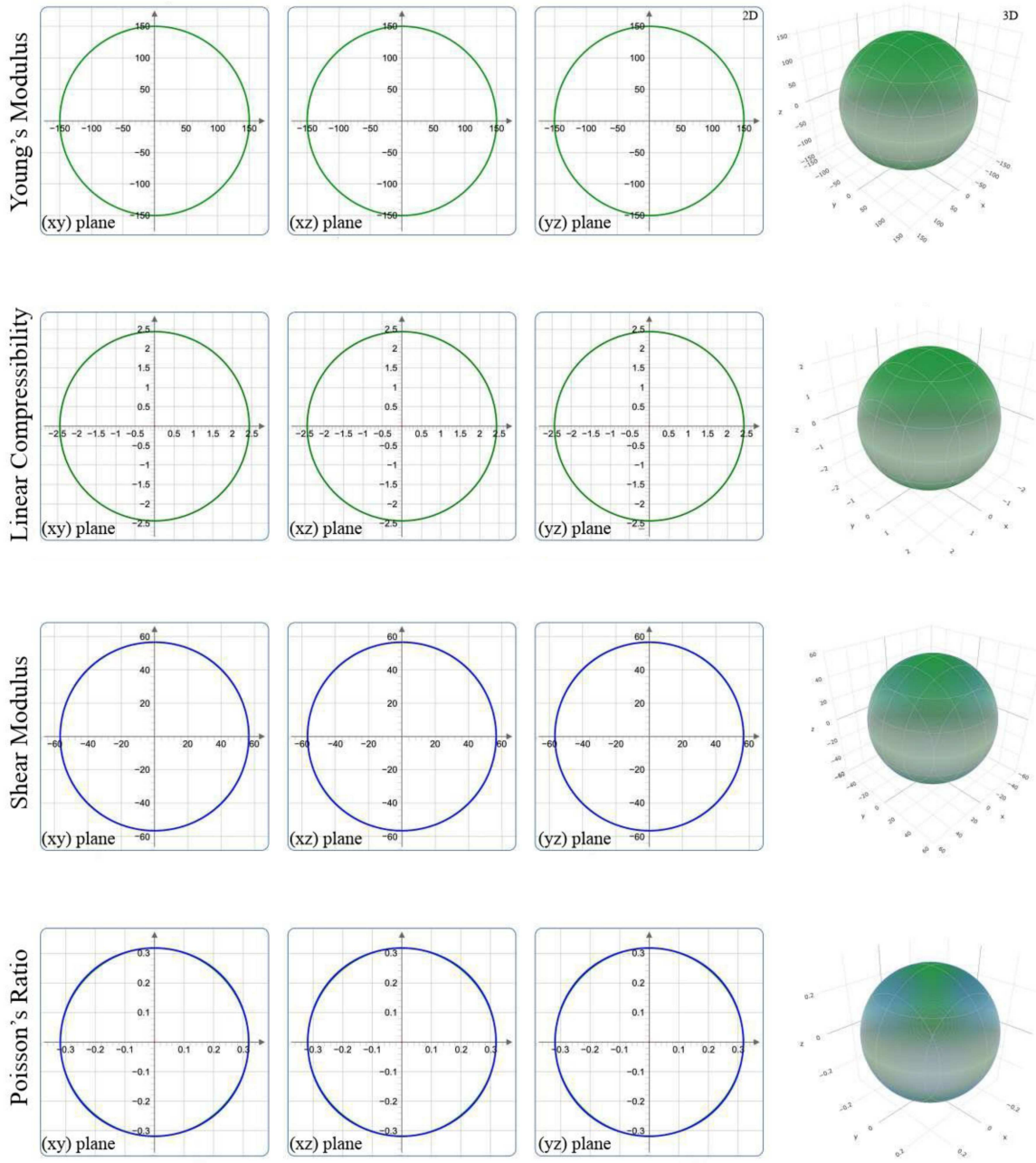

Fig. 5. Young's modulus, linear compressibility, shear modulus, and Poisson's ratio for $RbAlO_3$ LDA calculation.

a local maximum for group velocities. Moreover, the phase velocities have comparable values to those of the group velocities. For polarization of the sound waves, pseudo-longitudinal polarization exists in the primary mode, while pseudo-transverse polarization occurs in the secondary ones. Power flow angles have a local minimum for both transverse and longitudinal waves. Enhancement factors have a similar structure in both phase and group velocities. Additionally, the other compounds investigated share common observations. Due to the space restrictions, the remaining results have been presented in Appendix A.

3.3. Anisotropic properties

Anisotropic characteristics are widely utilized to assess the direction dependence of a compound. Furthermore, it allows forecasting microcracks that may arise in mechanical uses. The maximum–minimum computation of polycrystalline properties such as Poisson's ratio, Young's modulus, bulk modulus, and shear modulus are gaining importance owing to mechanical employment. Thereby, the boundary conditions of the compound are also determined. These parameters of compounds considered have been enumerated in Tables III and IV.

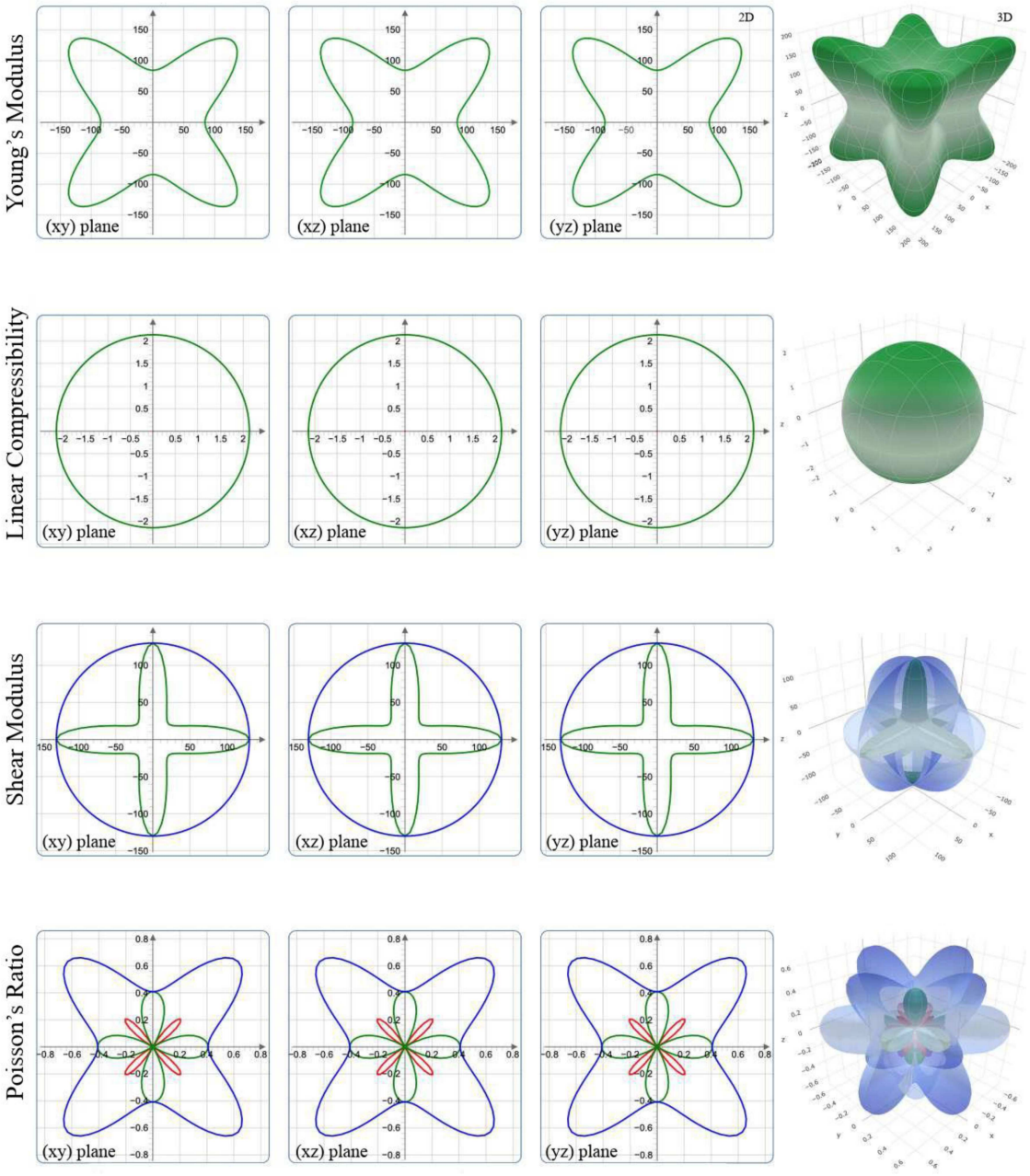

Fig. 6. Young's modulus, linear compressibility, shear modulus, and Poisson's ratio for $RbSiO_3$ GGA calculation.

As detailed in Table III, it is possible to say that the linear compressibility of these compounds does not have anisotropic behavior due to those maximum–minimum points being equal. Moreover, the related plots in Fig. 5 and 6 also confirms the same situation. It is a known fact that Poisson's ratio results must be between -1.0 and 0.5 [44]. The the remaining properties related to each plot are described in Appendix B. The Poisson's ratios $\nu_{\max}$ of $KAlO_3$ and $RbSiO_3$ are higher than the upper limit of Poisson's ratio, but $\nu_{\min}$ of those compounds are inside these limitations nonetheless. Hence, it is probable that these compounds demonstrate large elastic deformation under the little strain applied. In addition to the results provided on $RbSiO_3$, the calculations of both types show negative $\nu_{\min}$. It is estimated that the longitudinal strain applied to these compounds will increase their cross–section area. As a result of these properties, they resemble compounds known as auxetic compounds [45], which have a negative Poisson ratio.

The Zener anisotropy factor (A) that is given by

$$A = \frac{2C_{44}}{C_{11} - C_{12}} \tag{7}$$

is the measure of how far compounds theoretically are from being isotropic. Zener proposed the criteria as follows: $A = 1$ for isotropic compound;

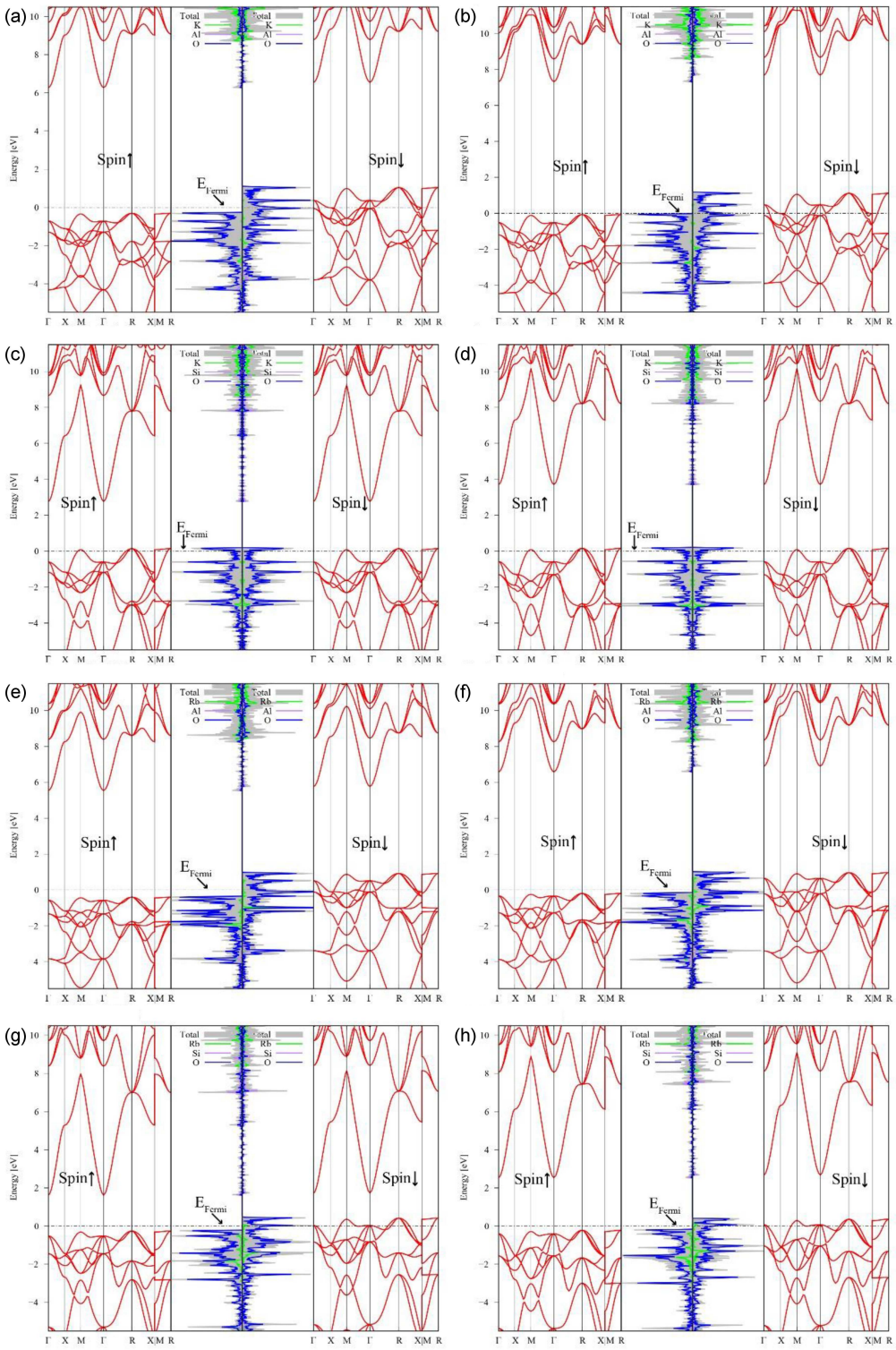

Fig. 7. The band structures and corresponding density of states (DOS) of (K, Rb)(Al, Si)O_3 perovskites (a) $KAlO_3$ GGA (b) $KAlO_3$ LDA (c) $KSiO_3$ GGA (d) $KSiO_3$ LDA (e) $RbAlO_3$ GGA (f) $RbAlO_3$ LDA (g) $RbSiO_3$ GGA (h) $RbSiO_3$ LDA.

$A \neq 1$ for anisotropic compound [46, 47]. These conditions are suitable for the formation of cubic crystals. As seen, a deviation of A greater than 1 leads to anisotropy. Zener's criteria were used to determine the anisotropy outcomes of the compounds investigated in this study. The obtained GGA (LDA) results are as follows: 0.284 (0.330) for $KAlO_3$, 1.714 (1.431) for $KSiO_3$, 1.175 (0.996) for $RbAlO_3$, 4.342 (3.591) for $RbSiO_3$. These results are presented in Table IV.

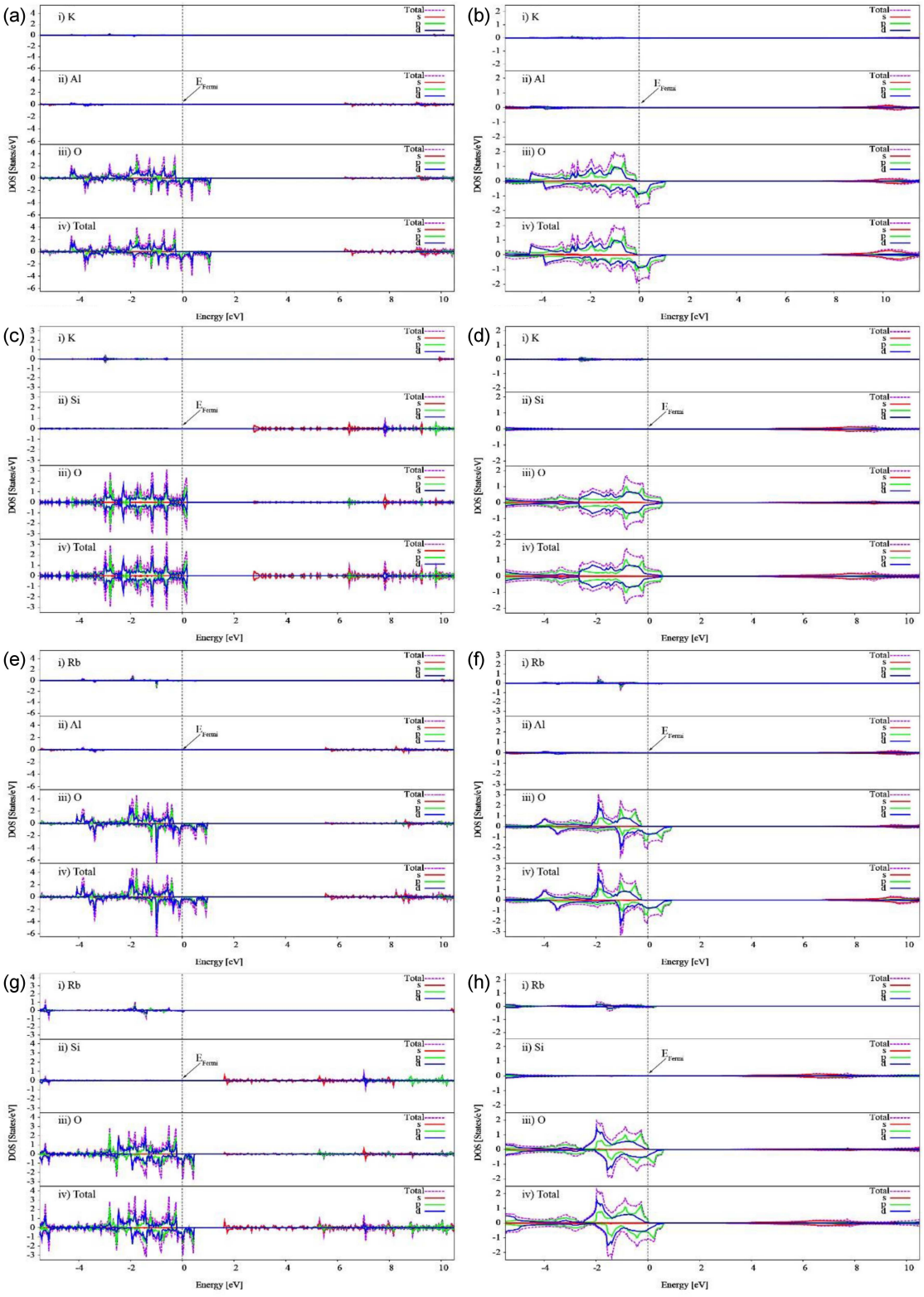

Fig. 8. The partial density of states (pDOS) of (K, Rb)(Al, Si)O_3 perovskites (a) $KAlO_3$ GGA (b) $KAlO_3$ LDA (c) $KSiO_3$ GGA (d) $KSiO_3$ LDA (e) $RbAlO_3$ GGA (f) $RbAlO_3$ LDA (g) $RbSiO_3$ GGA (h) $RbSiO_3$ LDA.

Consequently, it is possible to perceive that $KSiO_3$ and $RbAlO_3$ exhibit anisotropic characteristics, whereas $KAlO_3$ shows anisotropic nature. The LDA calculation of $RbAlO_3$ indicates an isotropic behavior, while the GGA result implies anisotropic behavior. By examining the plots related to these results, it can be concluded that $RbAlO_3$ has a relatively isotropic nature. In addition, these

distinctions in the Zener ratio of $RbAlO_3$ are assessed as being due to the preferred approximation. To the best of our knowledge, there is no experimental research to compare our calculation against in the literature.

The Debye temperature (θ_D), which is given by

$$\theta_D = \frac{h}{k_B}\left(\frac{3n}{4\pi}\frac{N_A\rho}{M}\right)^{1/3} V_m, \tag{8}$$

where

$$V_m = \left[\frac{1}{3}\left(\frac{2}{V_t^3}+\frac{1}{V_l^3}\right)\right]^{-1/3}, \tag{9}$$

$$V_l = \left(\frac{3B+4G}{2\rho}\right)^{1/2}, \tag{10}$$

$$V_t = \left(\frac{G}{\rho}\right)^{1/2}, \tag{11}$$

is an essential property for compounds since it is connected to thermal conductivity and melting temperature, as shown in Table IV. If the compounds have a high Debye temperature, they have high thermal conductivity and melting temperatures; otherwise, they have low thermal conductivity and melting temperatures. As detailed in Table IV, in the calculation of both types, $KSiO_3$ has a high θ_D, and $RbAlO_3$ has a low one. Thus, it is likely that $KSiO_3$ has high thermal conductivity and melting temperature, whereas $RbAlO_3$ has low ones.

3.4. Electronic properties

An investigation and discussion of a compound's electronic characteristics can reveal its electronic behavior. Hence, it is necessary to execute band calculations about related compounds. The obtained band structures and corresponding density of states (DOS) have been demonstrated in Fig. 7 by detailing both spin-up and spin-down.

As can be concluded from Figs. 7 and 8, the spin-up phases of both $KAlO_3$ calculations display semiconductor features, whereas the spin-down stages indicate metallic behavior. Several bands arising from O p–d states surpass the Fermi level in spin-down states, lending the compound a metallic character. When each $KSiO_3$ calculation is examined, it it can be seen that that O p–d states pass the Fermi level. Here, there is no shifting, such as in the case of $KAlO_3$, because no examination of $KSiO_3$ has magnetic moments calculated. $KSiO_3$ has a metallic character, since some bands emerge from O p–d states beyond the Fermi threshold in spin-down states. Except for $KSiO_3$, the magnetic moments of the investigated compounds are approximately as follows: for both $KAlO_3$ and $RbAlO_3$ (within GGA and LDA) $\mu \approx 2\ \mu_B$; for $RbSiO_3$ $\mu \approx 1\ \mu_B$. Except for $KSiO_3$, the magnetic moments of the investigated compounds are approximately as follows: for both $KAlO_3$ and $RbAlO_3$ (within GGA and LDA) $\mu \approx 2\ \mu$B; for $RbSiO_3$ $\mu \approx 1\ \mu$B. A few bands arising from O p–d down states outrun the Fermi level, and this causes the the metallic behavior. Consequently, $KAlO_3$, $RbAlO_3$, and $RbSiO_3$ likely have half-metallicity properties since their O p–d down states exceed the Fermi level, but unlike them, $KSiO_3$ likely has metallic properties too, due to both states overtaking the Fermi level. Furthermore, as the spin-up states approach the Fermi level, they shift to the spin-down states, and this draws attention to the half-metallicity properties of present compounds. In addition, the current shifts observed are thought to be due to their magnetic moments. Furthermore, these compounds' spin-up band structure and states, except for $KSiO_3$, are semiconducting gaps. The calculated GGA (LDA) band gaps are as follows: 7.020 (7.403) eV for $KAlO_3$; 6.111 (6.915) eV for $RbAlO_3$; 2.150 (2.947) eV for $RbSiO_3$. On the other hand, the spin-down differences are metallic. In addition, the calculated GGA (LDA) half-metallic band gaps are as already follows: 1.040 (1.120) eV for $KAlO_3$; 0.930 (0.980) eV for $RbAlO_3$; 0.420 (0.365) eV for $RbSiO_3$. From this perspective, it can be regarded as another sign of these compounds' half-metallic characteristics.

According to the pDOS plots of the GGA (LDA) calculation of $KAlO_3$ in Fig. 8, the K addition is small in the examined range. Before the Fermi level, the Al contribution is low, but beyond the Fermi level, the increase of Al-s is at nearly 6 (8) eV. The O contribution is from -4 (-4) eV to the Fermi level. Moreover, the O contribution begins at 6 (8) eV after the Fermi level. For $KSiO_3$, the K donation is found at both -3 (-2) eV and 10 eV. The Si contribution is limited before the Fermi threshold, whereas it is established at around 2.5 (4) eV away from the threshold. From -5.5 eV to the Fermi level, the O addition is detected and cuts the level. It is distinguished from around 2.5 (4) to 10.5 eV. As $RbAlO_3$, the Rb donation barely appears at about -1 (-1) eV. The Al contribution is tiny until the Fermi level, but after the Fermi level, the increase of Al-s is about 5.5 (7.5) eV. The influence of O ranges from -4 (-4.5) eV to the Fermi level. Furthermore, the O contribution starts at 8 (9) eV after the Fermi level. Regarding $RbSiO_3$, the Rb contribution can be observed at both -5 (-5) eV and -2.5 (-2) eV. Until the Fermi restriction, the Si contribution is modest after probably -5 (-4.5) eV, but it becomes significant after about 1.75 (2.5) eV. The O addition is observed from -5.5 eV to the Fermi level. Beyond the Fermi threshold, it increases from 1.75 (4) to 10.5 eV. Apart from $KSiO_3$, which has no magnetic moment, the observed differences in each spin-up and spin-down state have resulted from the magnetic character of the present compounds. Furthermore, it might be concluded that it is the indicator of the half-metallicity of the compounds discussed.

The electron-density patterns of considered compounds have been obtained to discuss electronic behavior, and Fig. 9 demonstrates the corresponding distribution in the (110) plane for compounds

TABLE V

The Bader net charges of (K, Rb)(Al, Si)O_3 perovskites.

Compounds	GGA				LDA			
	$KAlO_3$	$KSiO_3$	$RbAlO_3$	$RbSiO_3$	$KAlO_3$	$KSiO_3$	$RbAlO_3$	$RbSiO_3$
K/Rb	0.79	0.76	0.79	0.77	0.77	0.75	0.79	0.76
Al/Si	2.84	3.65	2.83	3.63	2.80	3.65	2.81	3.62
O	−3.63	−4.41	−3.62	−4.40	−3.57	−4.50	−3.60	−4.38

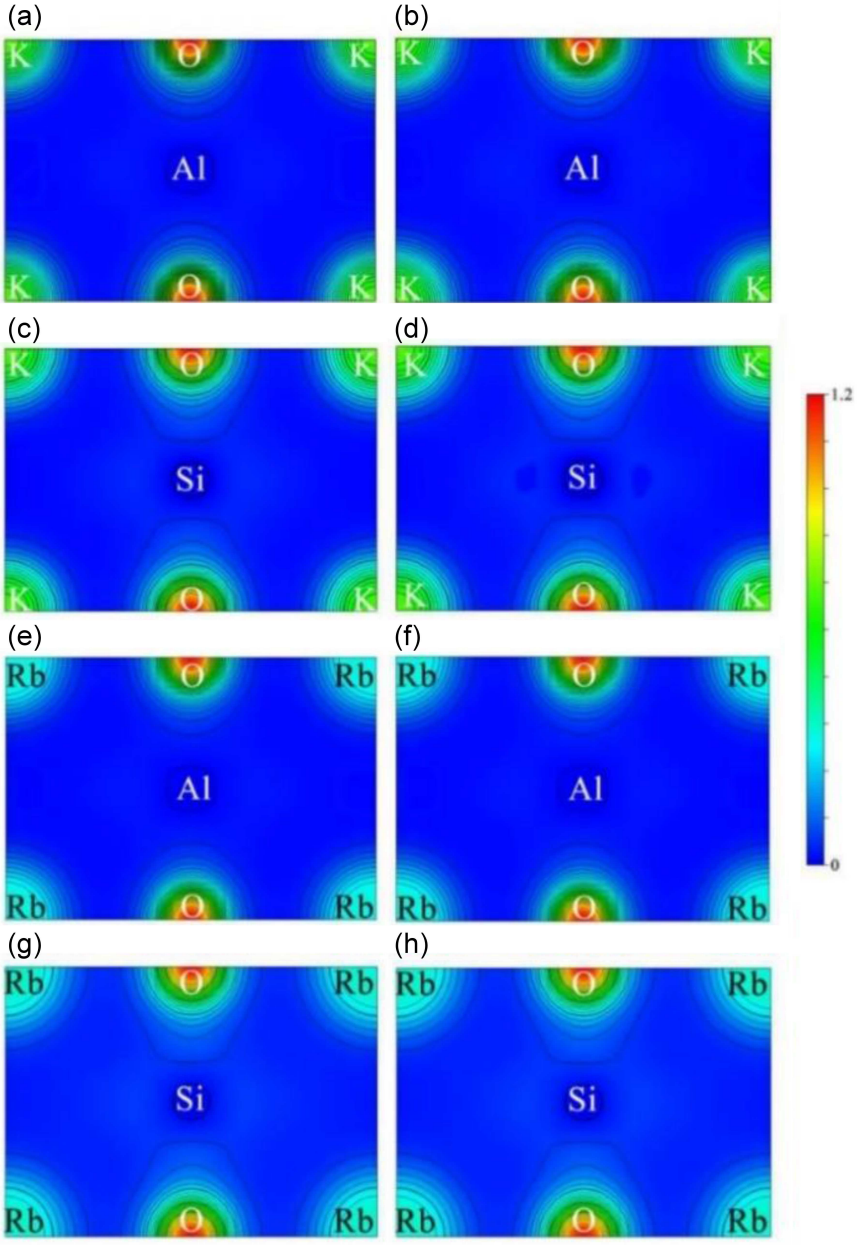

Fig. 9. The electron–density patterns of (K, Rb)(Al, Si)O_3 perovskites (a) $KAlO_3$ GGA (b) $KAlO_3$ LDA (c) $KSiO_3$ GGA (d) $KSiO_3$ LDA (e) $RbAlO_3$ GGA (f) $RbAlO_3$ LDA (g) $RbSiO_3$ GGA (h) $RbSiO_3$ LDA.

under consideration. Existing compounds, as shown in Fig. 9, have dominantly ionic properties, which aligns with the results of Poisson's and G/B ratios in Table II. Moreover, the charge displacement of current compounds, as demonstrated in Table V, has been obtained in this article using the Bader partial charge algorithm [48] executed by the Henkelman group [49]. Here, negative net charges indicate delivery of charges to the atom, while positive ones indicate delivery from the bit. As deduced from Table V, the atoms K, Rb, Al, and Si can be assumed to constitute delivery charges because of

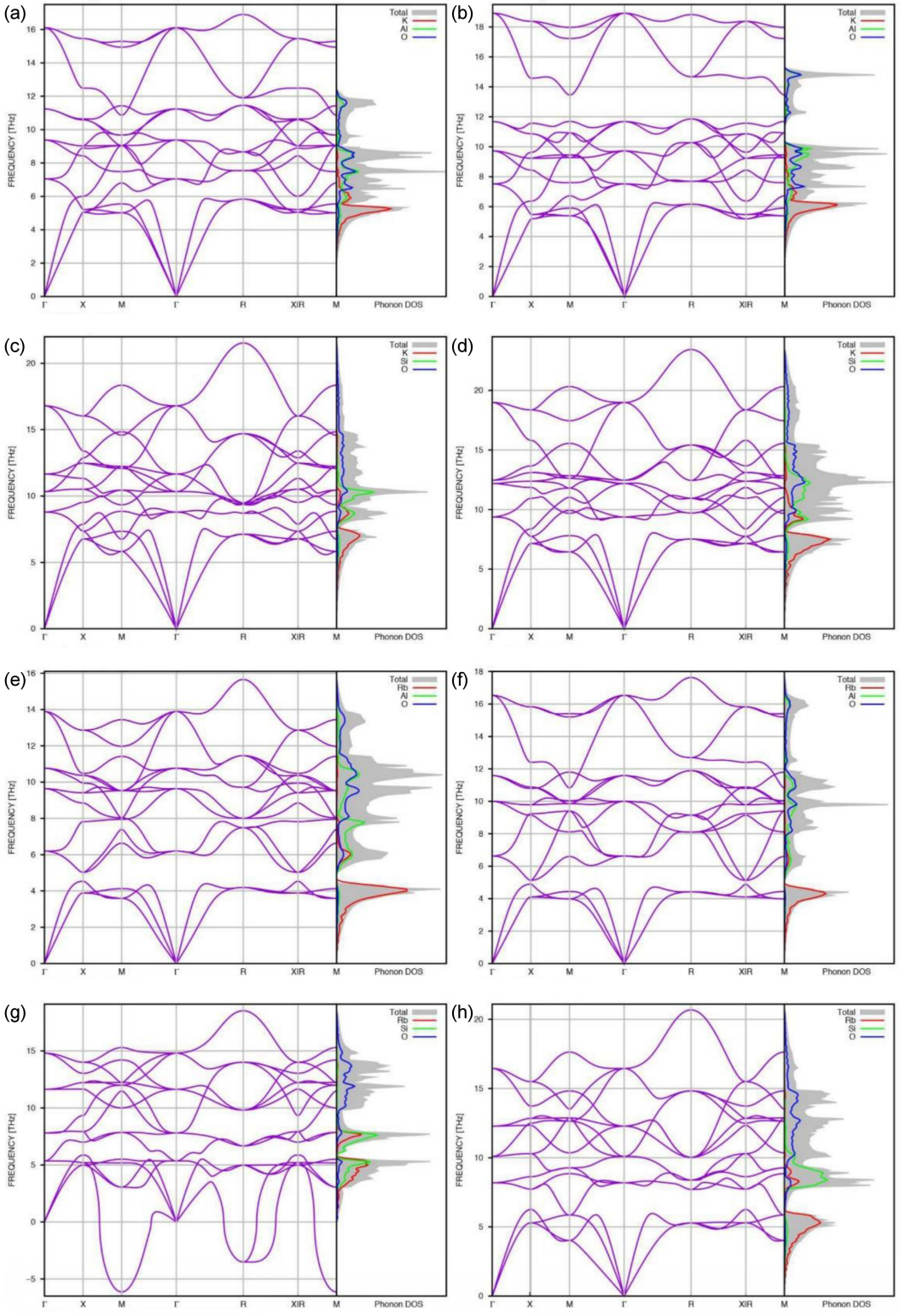

Fig. 10. The calculated phonon dispersion curves and related phonon density of states (PDOS) of (K, Rb)(Al, Si)O_3 perovskites (a) $KAlO_3$ GGA (b) $KAlO_3$ LDA (c) $KSiO_3$ GGA (d) $KSiO_3$ LDA (e) $RbAlO_3$ GGA (f) $RbAlO_3$ LDA (g) $RbSiO_3$ GGA (h) $RbSiO_3$ LDA.

their positive net charges. However, O atoms have negative charges. In a nutshell, it is reasonable to conclude that the charge is transferred from atoms K, Rb, Al, and Si to atom O for each compound. Along with these results, as seen in Table V, the total charges for each compound analyzed are zero.

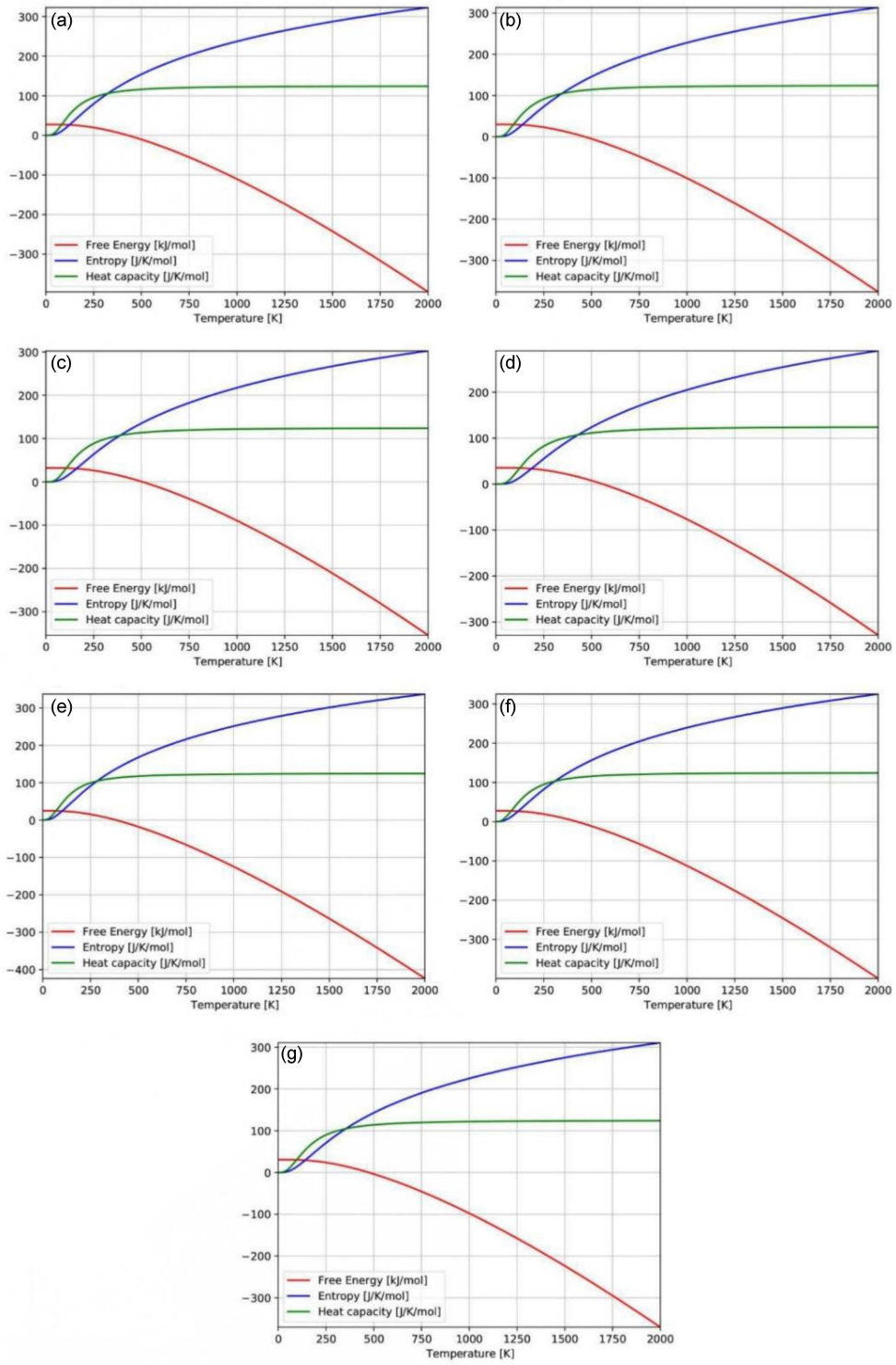

Fig. 11. The calculated thermal properties of (K, Rb)(Al, Si)O_3 perovskites (a) $KAlO_3$ GGA (b) $KAlO_3$ LDA (c) $KSiO_3$ GGA (d) $KSiO_3$ LDA (e) $RbAlO_3$ GGA (f) $RbAlO_3$ LDA (g) $RbSiO_3$ LDA.

3.5. Lattice dynamical and thermodynamical properties

Figure 10 demonstrates phonon dispersion curves and related density of states (DOS) for each compound under investigation. In line with observations, it it can be noted that there are fifteen phonon branches, owing to five atoms found in their unit cell. Hence, twelve of these branches are optical modes, whereas the rest are acoustic modes. In addition, the compounds investigated are dynamically stable, except for $RbSiO_3$ GGA, which has

a negative frequency. Concurrently, it can be observed that the K and Rb atoms are dominant at low frequencies, the Al and Si atoms are dominant at frequencies greater than K and Rb, and the O atoms are predominant at high frequencies. These differences are probably a result of the fact that elements have different masses.

The thermal properties of compounds under investigation have been discussed using the quasi-harmonic approach. Except for $RbSiO_3$ GGA, which has negative frequencies, Fig. 11 depicts the thermal characteristics of each of the compounds. These visualizations show free energy, entropy, and heat capacity as a function of temperature. Furthermore, it is visible that the free energy exponentially decreases as the temperature increases. On the other hand, the entropy increases accordingly as the temperature rises. At low temperatures, heat capacity increases dramatically, and at high temperatures, it hits a constant known as the Dulong–Petit limit.

4. Conclusions

The goal of this investigation was to review the structural, elastic, anisotropic elastic, electronic, and lattice dynamical properties of (K, Rb)(Al, Si)O_3 perovskites using first-principles calculations with VASP version 544. Also, in view of the computed negative formation enthalpy, this essay revealed that the optimized structures of the compounds under investigation are both thermodynamically stable and experimentally synthesizable. $KSiO_3$ is the most decisive among the compounds studied because it has the lowest negative formation energy. In addition, in line with computations, $KSiO_3$ has the lowest lattice parameter, while $RbAlO_3$ has the biggest one. The LDA investigation of $KAlO_3$ is the ferromagnetic phase, but GGA is anti-ferromagnetic. These contradictions could be assessed as the result of the selected approximation. In addition, the characteristics of $KSiO_3$ are parallel. For each calculation type, $RbAlO_3$ and $RbSiO_3$ have ferromagnetic phases. It can be noted that compounds under examination fulfill the Born mechanical stability criteria. The polycrystalline properties, such as Young's, bulk, shear moduli, and Poisson's ratio, have been determined for each. Accordingly, polycrystalline properties have demonstrated that $KSiO_3$ has the highest Young's, bulk, and shear moduli, while $RbAlO_3$ has the smallest ones. Consistent with these compounds, based on both their C_p and B/G results, it is reasonable to say that $KSiO_3$ exhibits brittle behavior, and the others demonstrate ductile behavior. Moreover, these compounds were evaluated as relatively hard since their H_ν's are less than 40 GPa. It is suspected that $KAlO_3$ and $RbSiO_3$ exhibit substantial elastic deformation at a little strain applied due to $\nu_{\max}$ being off-limits. Since $RbSiO_3$ has a negative $\nu_{\min}$, it is expected that applying longitudinal strain to these compounds will increase their cross-sectional area. The anisotropy results have argued that $RbAlO_3$ has a comparatively isotropic character, while the others have anisotropic nature. Since each $KSiO_3$ calculation has a high Debye temperature, $KSiO_3$ has both a high melting temperature and a high thermal conductivity. As for investigated electronic properties, $KAlO_3$, $RbAlO_3$, and $RbSiO_3$ have shown half-metallic nature. However, $KSiO_3$ has exhibited metallic characteristics. Except for $KSiO_3$, others have magnetic moments as follows: within GGA and LDA for $KAlO_3$ and $RbAlO_3$ $\mu \approx 2\ \mu_B$; for $RbSiO_3$ $\mu \approx 1\ \mu_B$. Moreover, these results are in line with the expected magnetic properties. Furthermore, it was discovered that the compounds under consideration demonstrate a dominantly ionic bonding nature. With the exception of the GGA calculation of $RbSiO_3$, other compounds are dynamically stable. Furthermore, the compounds discussed turned out to be compounds full of potential due to their mechanical, thermodynamic, and dynamic properties disclosed in this study. Finally, this article can assist in a better understanding of these compounds and their properties and motivate further experimental research.

Acknowledgments

This study was carried out with products from 0362–NAP16, 0147–NAP12, and 0790–DR–21 projects financed and supported by Burdur Mehmet Akif Ersoy University. The authors, therefore, thank Burdur Mehmet Akif Ersoy University for technical and financial support and NanoSim Laboratory for the use of HPC Systems.

Appendix

A: Mechanical properties

The calculated mechanical properties of the considered compounds are listed below (see Figs. 12–17).

B: Anisotropic properties

The calculated anisotropic properties of the remaining compounds are listed below (see Figs. 18–23).

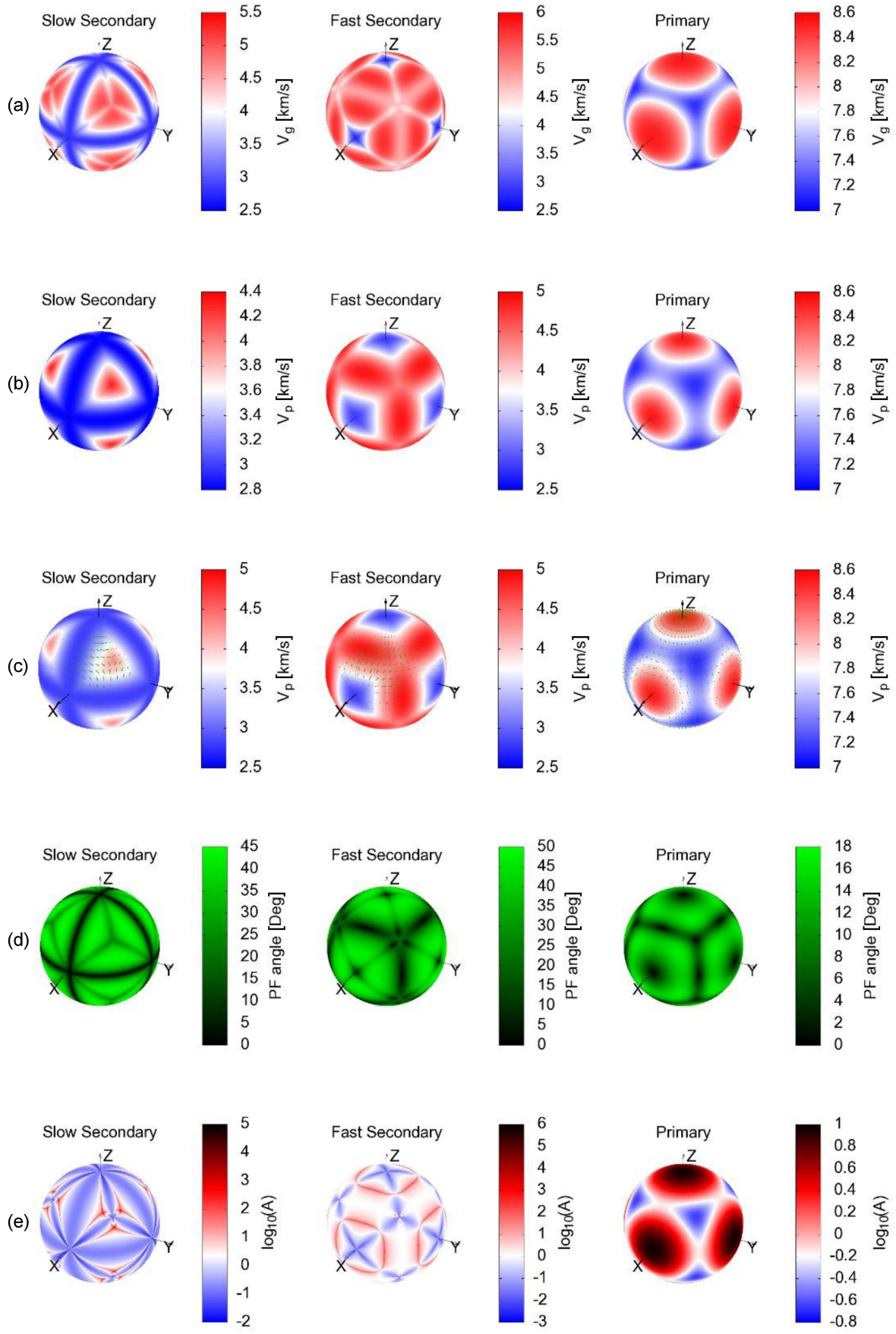

Fig. 12. (a) Group and (b) phase velocities, (c) polarization of sound waves, (d) power flow angles, and (e) enhancement factors for $KAlO_3$ LDA calculation.

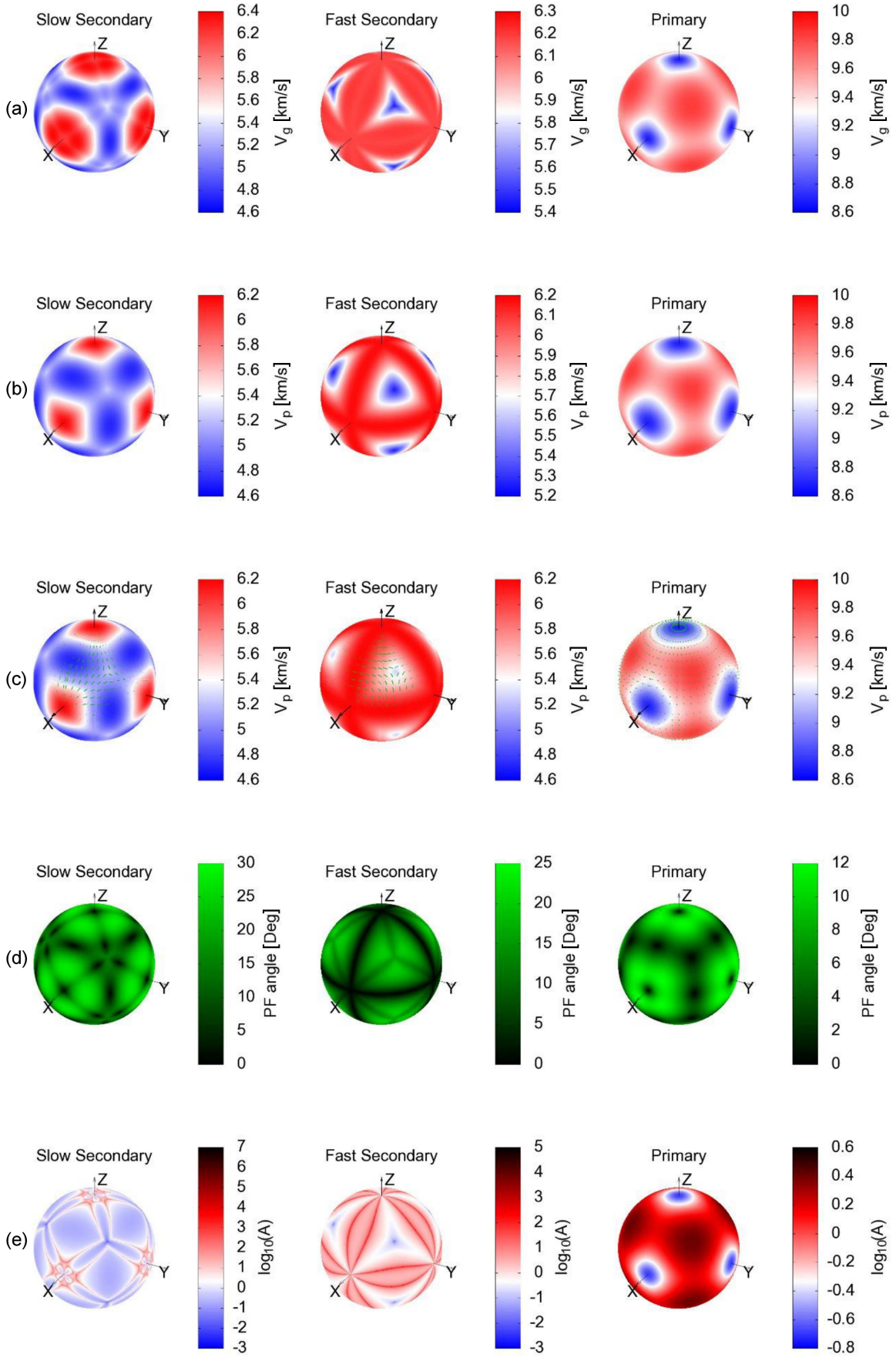

Fig. 13. (a) Group and (b) phase velocities, (c) polarization of sound waves, (d) power flow angles, and (e) enhancement factors for $KSiO_3$ GGA calculation.

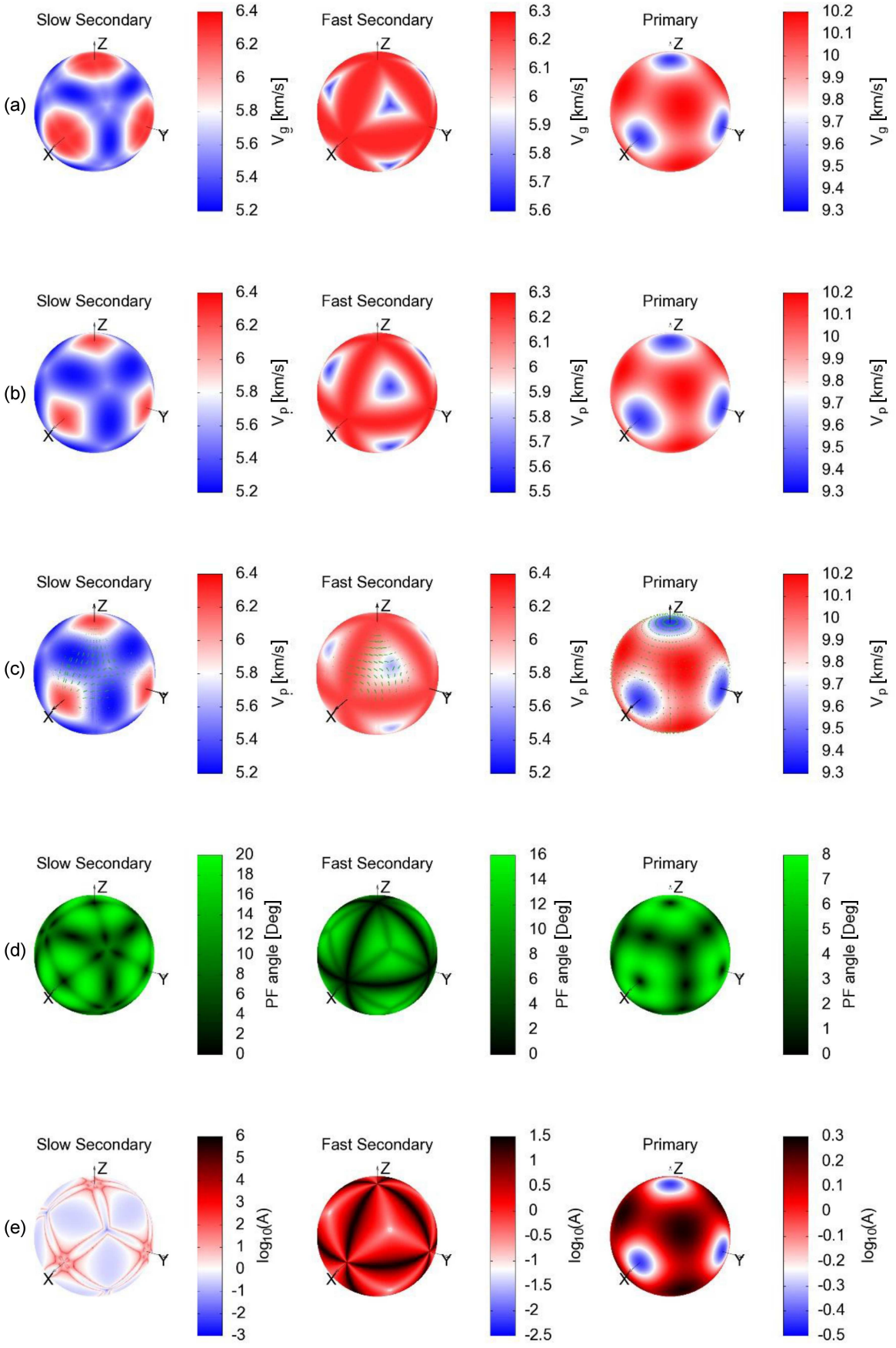

Fig. 14. (a) Group and (b) phase velocities, (c) polarization of sound waves, (d) power flow angles, and (e) enhancement factors for $KSiO_3$ LDA calculation.

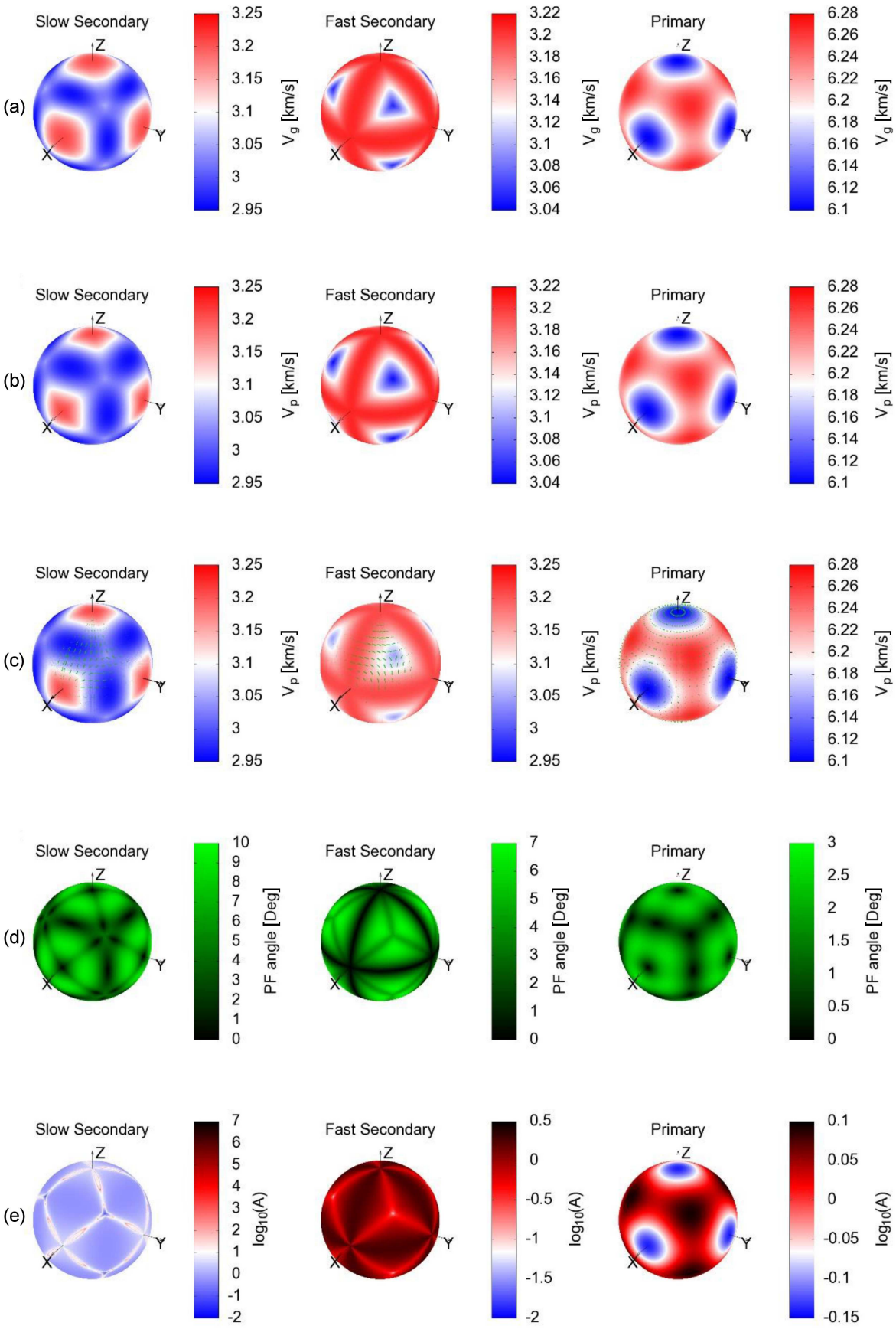

Fig. 15. (a) Group and (b) phase velocities, (c) polarization of sound waves, (d) power flow angles, and (e) enhancement factors for $RbAlO_3$ GGA calculation.

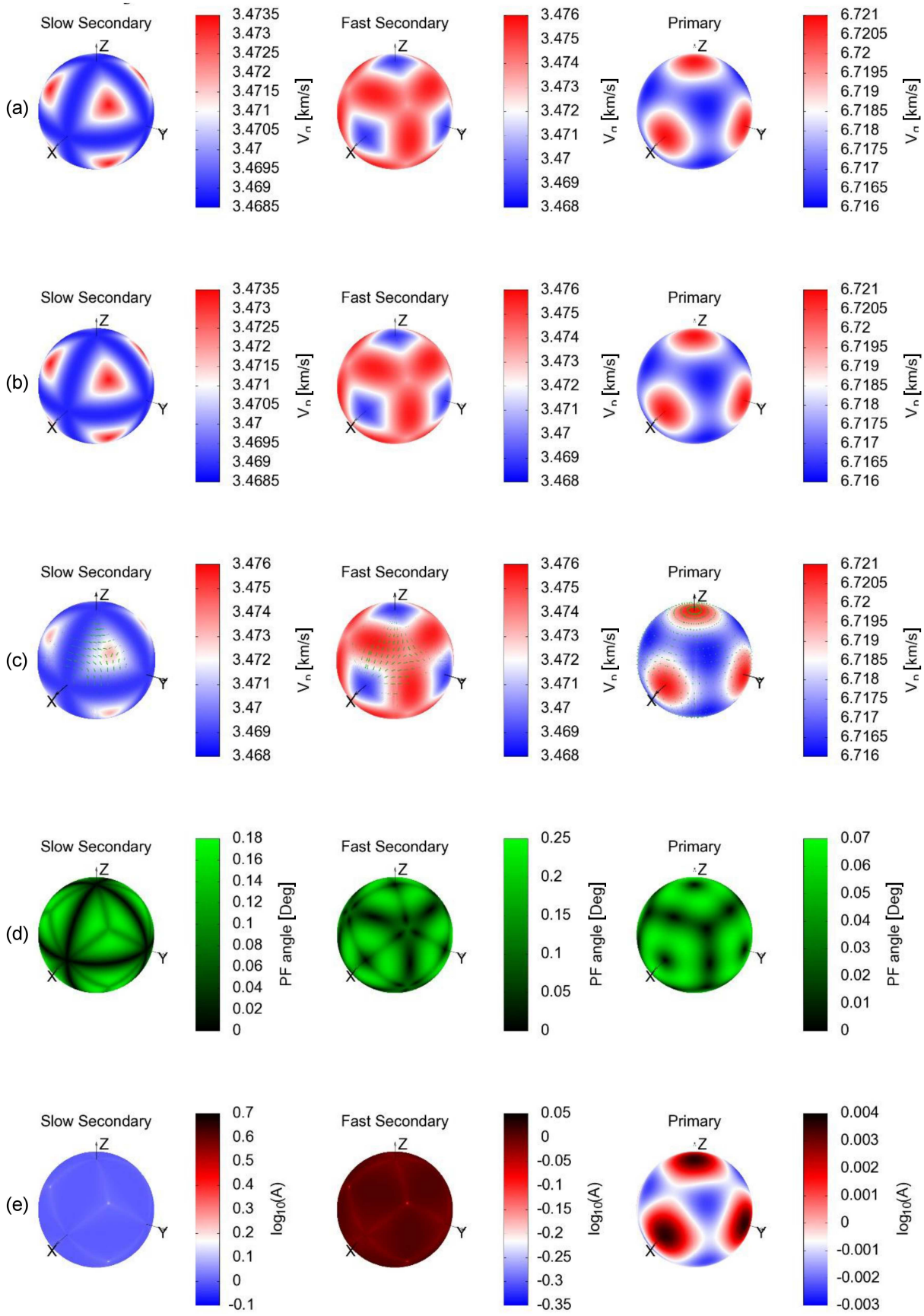

Fig. 16. (a) Group and (b) phase velocities, (c) polarization of sound waves, (d) power flow angles, and (e) enhancement factors for $RbAlO_3$ LDA calculation.

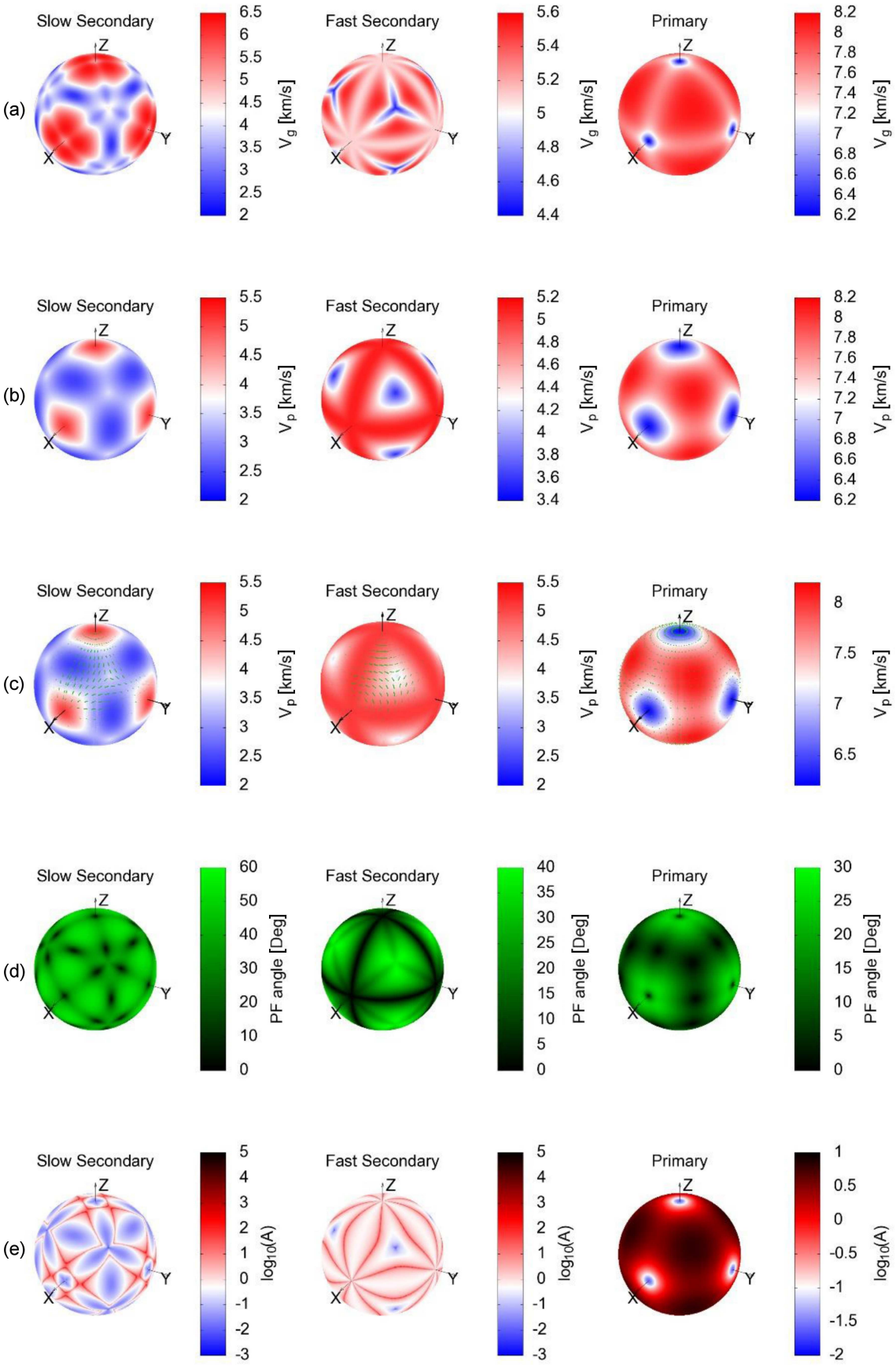

Fig. 17. (a) Group and (b) phase velocities, (c) polarization of sound waves, (d) power flow angles, and (e) enhancement factors for $RbSiO_3$ GGA calculation.

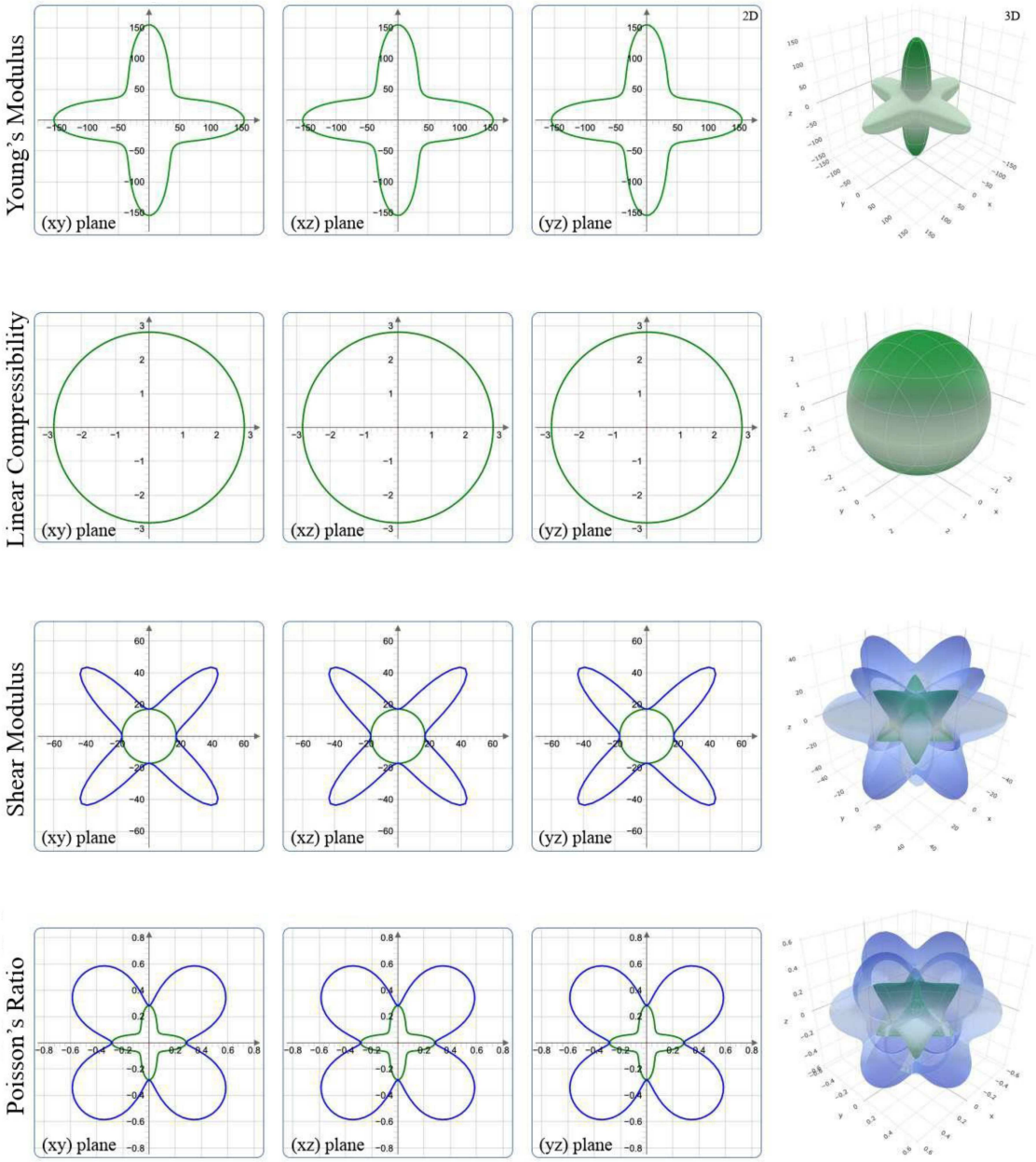

Fig. 18. Young's modulus, linear compressibility, shear modulus, and Poisson's ratio for $KAlO_3$ GGA calculation.

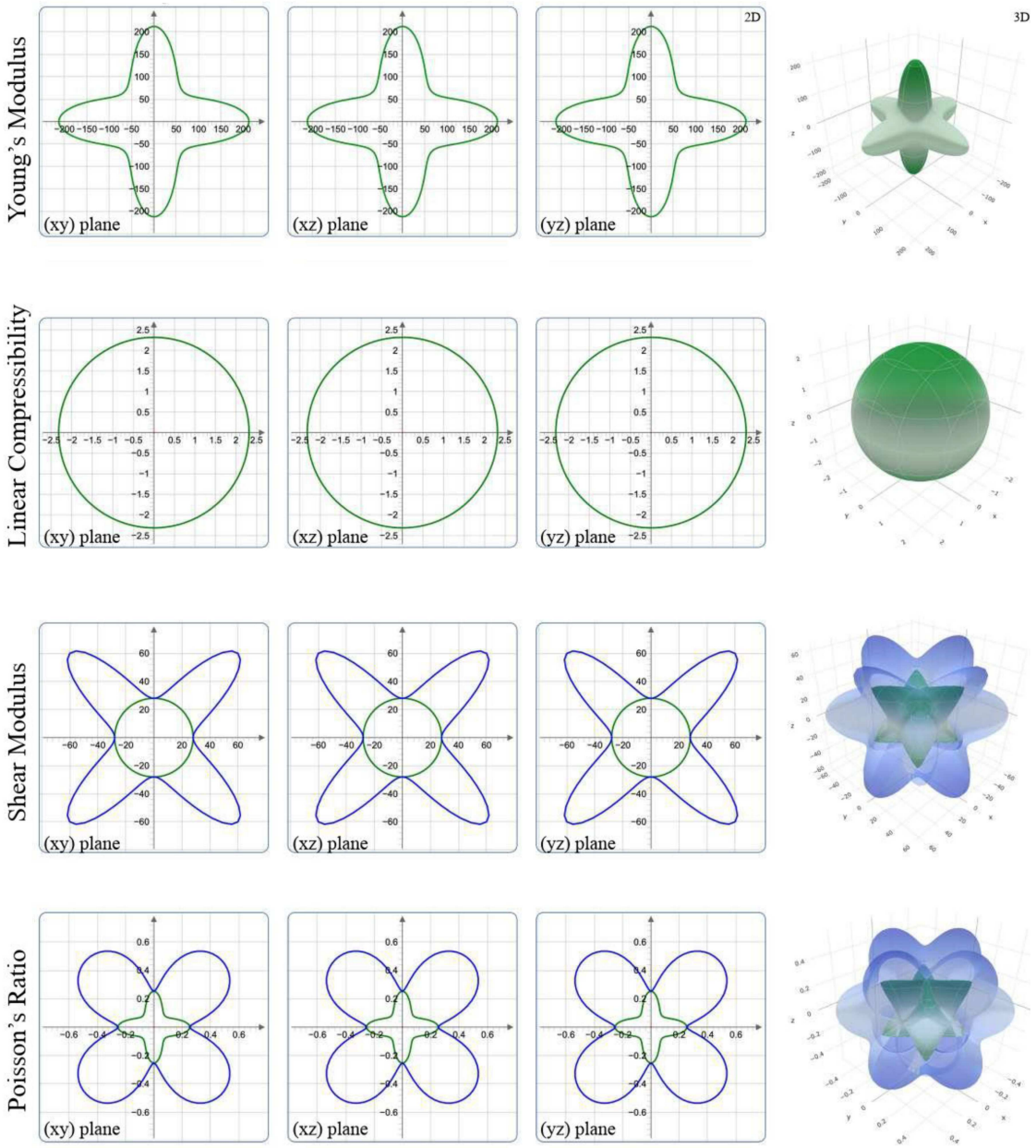

Fig. 19. Young's modulus, linear compressibility, shear modulus, and Poisson's ratio for $KAlO_3$ LDA calculation.

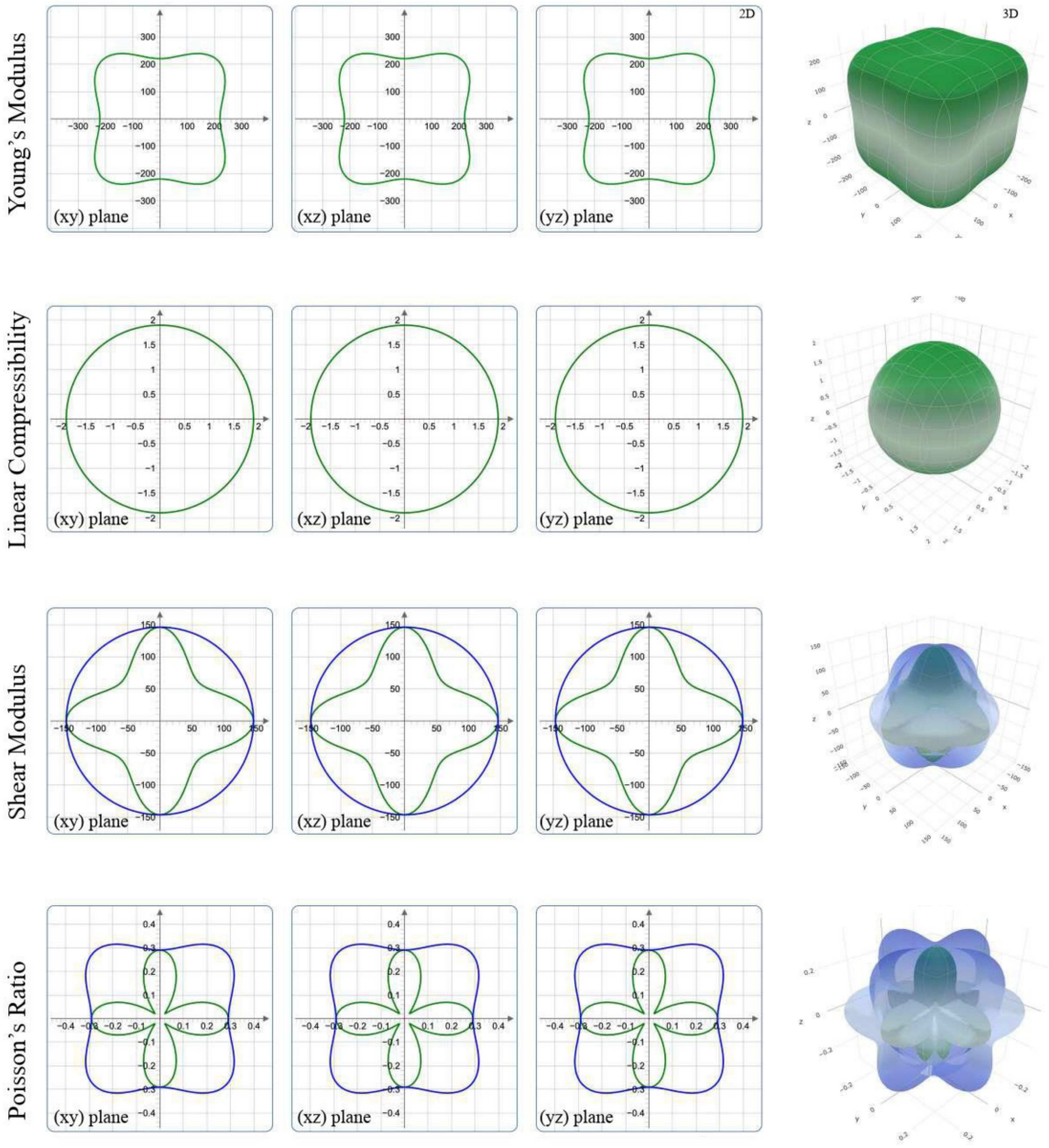

Fig. 20. Young's modulus, linear compressibility, shear modulus, and Poisson's ratio for $KSiO_3$ GGA calculation.

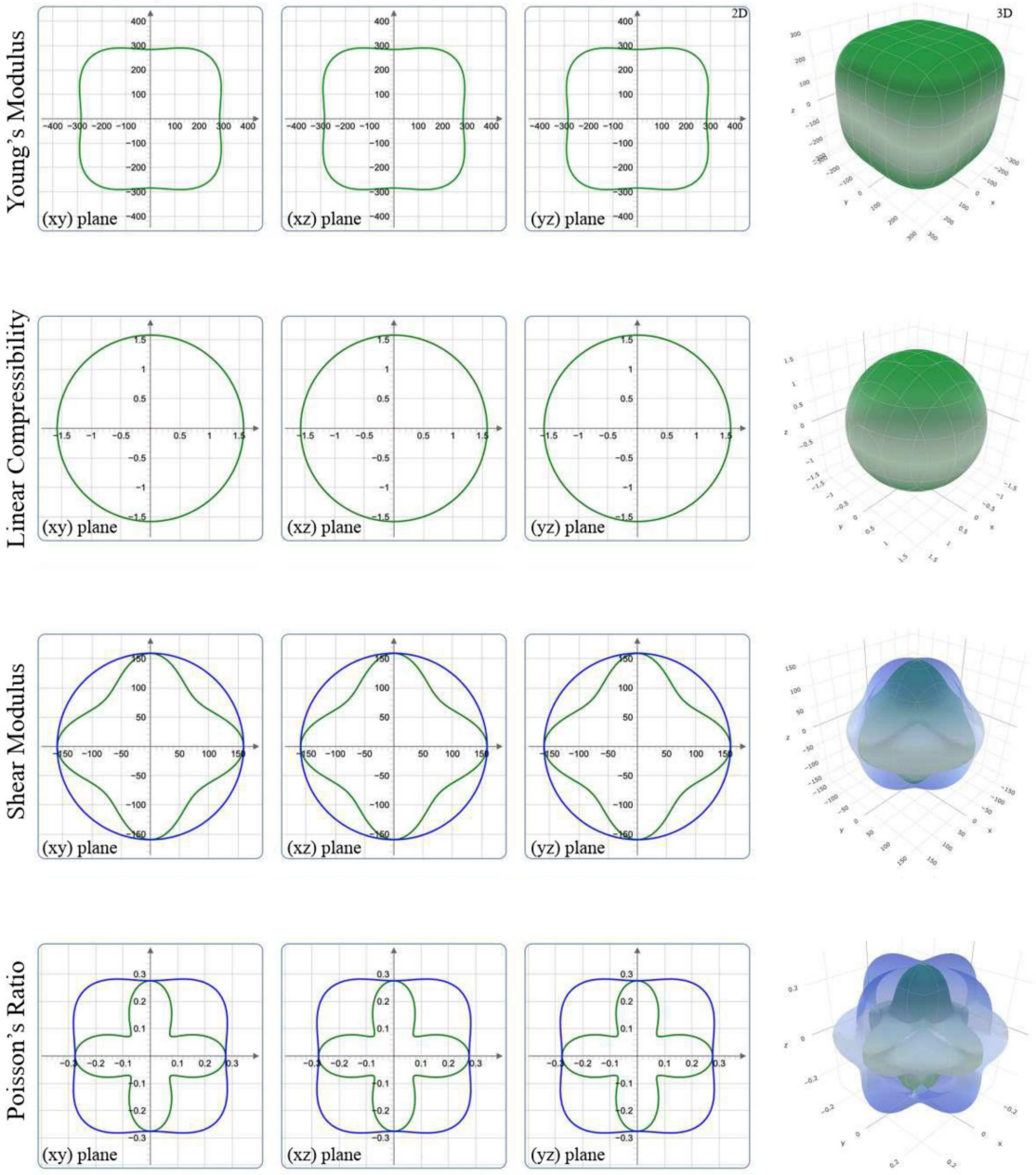

Fig. 21. Young's modulus, linear compressibility, shear modulus, and Poisson's ratio for $KSiO_3$ LDA calculation.

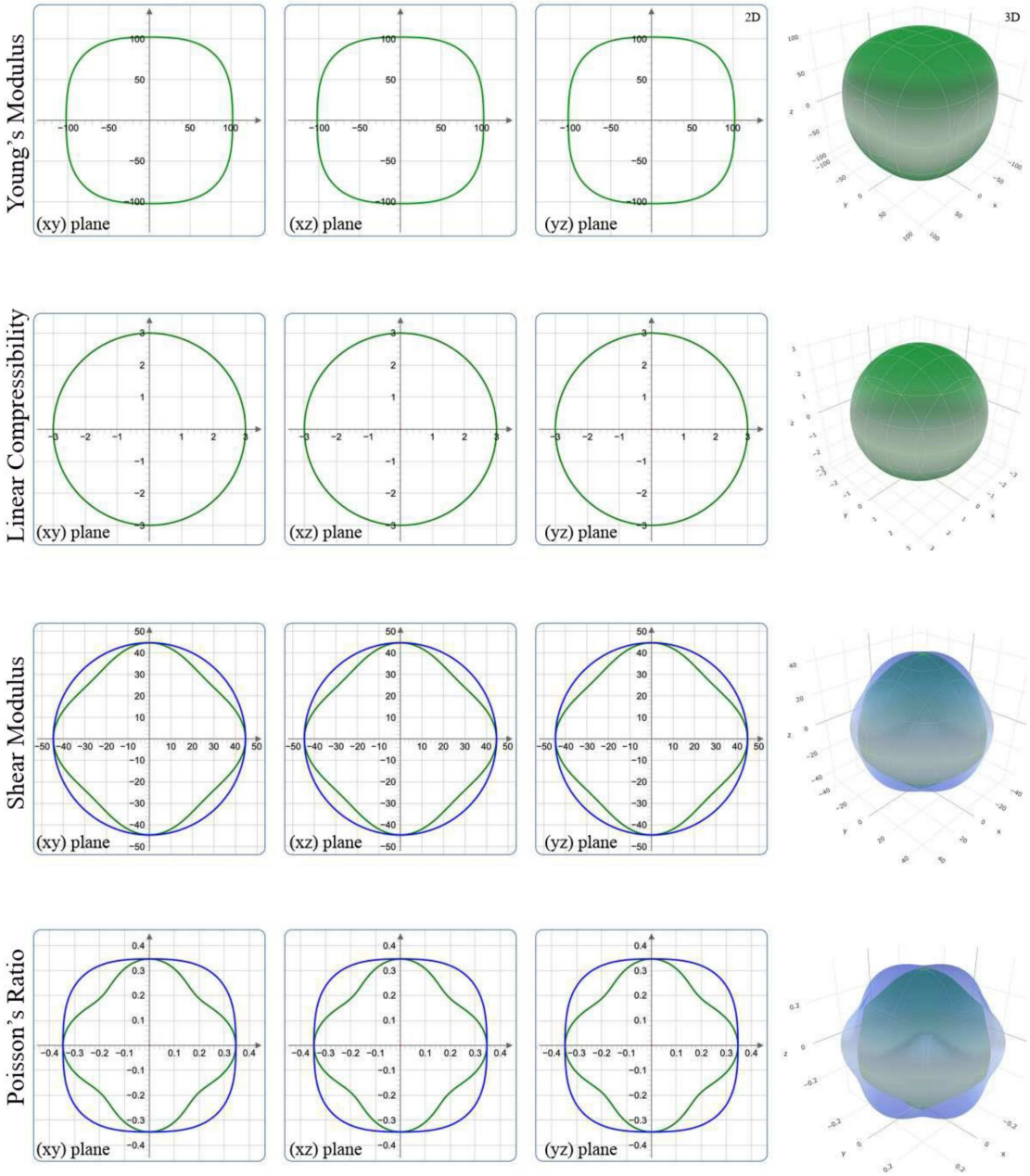

Fig. 22. Young's modulus, linear compressibility, shear modulus, and Poisson's ratio for $RbAlO_3$ GGA calculation.

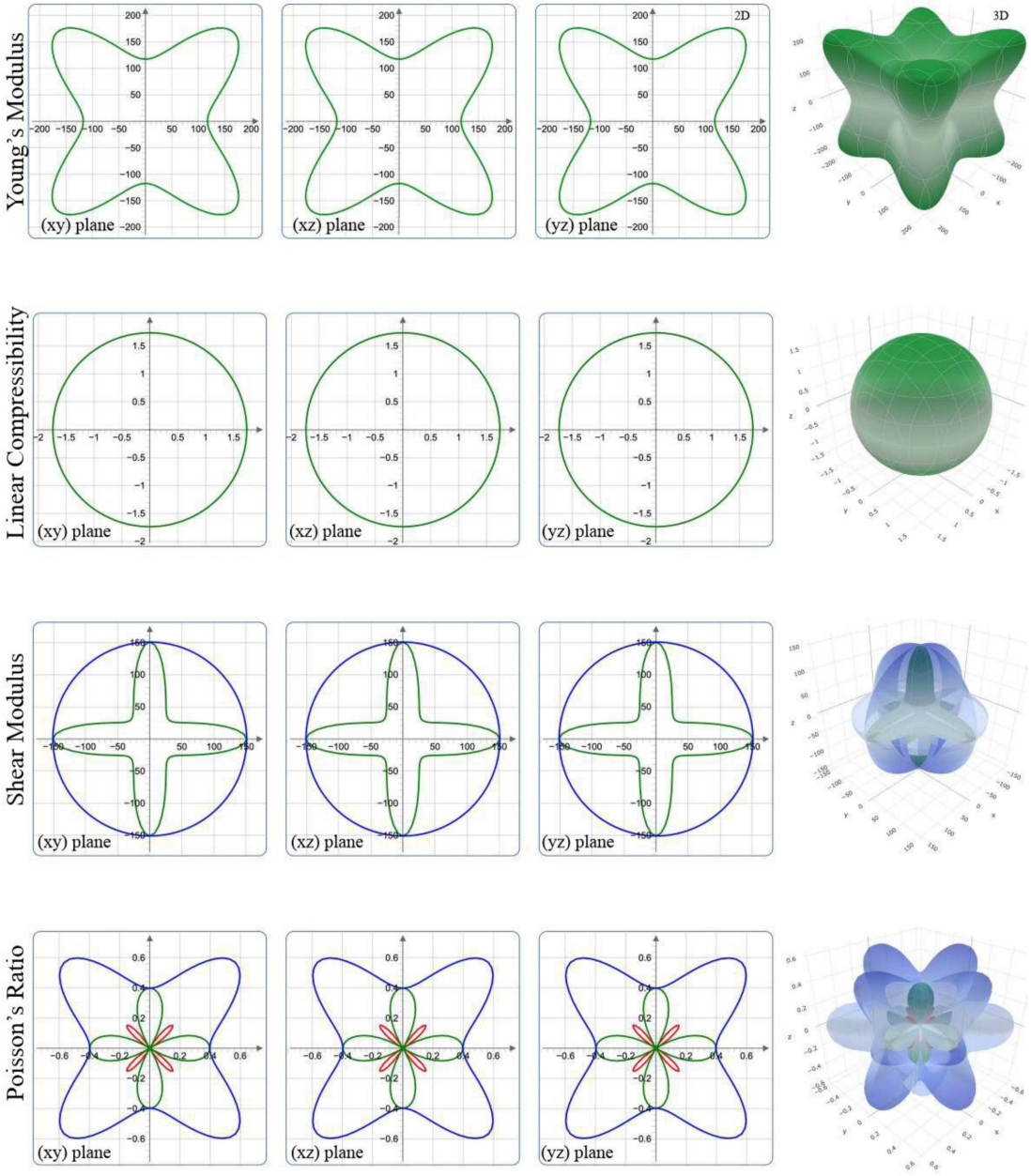

Fig. 23. Young's modulus, linear compressibility, shear modulus, and Poisson's ratio for $RbSiO_3$ LDA calculation.

References

[1] H. Absike, N. Baaalla, L. Attou, H. Labrim, B. Hartiti, H. Ez-zahraouy, *Solid State Commun.* **345**, 114684 (2022).

[2] N.-G. Park, *Materials Today* **18**, 65 (2015).

[3] W. Yu, D. Zhou, T. Zhou, Y. Tian, X. Zhu, Y. Tu, *J. Nanomater.* **2018**, 8148072 (2018).

[4] K. Yao, F. Li, Q. He, X. Wang, Y. Jiang, H. Huang, A.K.-Y. Jen, *Nano Energy* **40**, 155 (2017).

[5] F. Calle-Vallejo, J. Martinez, J.M. Garcia-Lastra, M. Mogensen, J. Rossmeisl, *Angew. Chem. Int. Ed.* **49**, 7699 (2010).

[6] A. Dutta, P.K. Mukhopadhyay, T.P. Sinha, D. Das, S. Shannigrahi, *Solid State Sci.* **58**, 64 (2016).

[7] V. Bannikov, *Mater. Chem. Phys.* **171**, 119 (2016).

[8] H. Rached, S. Bendaoudia, D. Rached, *Mater. Chem. Phys.* **193**, 453 (2017).

[9] J. Hwang, Z. Feng, N. Charles et al., *Mater. Today* **31**, 100 (2019).

[10] M. Wu, X. Lou, T. Li, J. Li, S. Wang, W. Li, B. Peng, G. Gou, *J. Alloys Compd.* **724**, 1093 (2017).

[11] A. Kumar, R. Jha, R.P. Tandon, V.P.S. Awana, *Solid State Commun.* **152**, 1678 (2012).

[12] J. Ihringer, J.K. Maichle, W. Prandl, A.W. Hewat, T. Wroblewski, *Z. Phys. B Condensed Matter* **82**, 171 (1991).

[13] Y. Moritomo, A. Asamitsu, H. Kuwahara, Y. Tokura, *Nature* **380**, 141 (1996).

[14] J.M. De Teresa, M.R. Ibarra, P.A. Algarabel, C. Ritter, C. Marquina, J. Blasco, J. Garcia, A. del Moral, Z. Arnold, *Nature* **386**, 256 (1997).

[15] S. Berri, *J. Sci. Adv. Mater. Devices* **3**, 254 (2018).

[16] H. Iwahara, H. Uchida, K. Ono, K. Ogaki, *J. Electrochem. Soc.* **135**, 529 (1988).

[17] A. Gencer, G. Surucu, *Int. J. Hydrogen Energy* **45**, 10507 (2020).

[18] G. Kresse, J. Furthmüller, *Phys. Rev. B* **54**, 11169 (1996).

[19] G. Kresse, J. Furthmüller, *Computat. Mater. Sci.* **6**, 15 (1996).

[20] P.E. Blöchl, *Phys. Rev. B* **50**, 17953 (1994).

[21] G. Kresse, D. Joubert, *Phys. Rev. B* **59**, 1758 (1999).

[22] J.P. Perdew, K. Burke, M. Ernzerhof, *Phys. Rev. Lett.* **77**, 3865 (1996).

[23] D.M. Ceperley, B.J. Alder, *Phys. Rev. Lett.* **45**, 566 (1980).

[24] J.P. Perdew, A. Zunger, *Phys. Rev. B* **23**, 5048 (1981).

[25] P.A.M. Dirac, *Math. Proc. Camb. Philos. Soc.* **26**, 376 (1930).

[26] H.J. Monkhorst, J.D. Pack, *Phys. Rev. B* **13**, 5188 (1976).

[27] M. Methfessel, A.T. Paxton, *Phys. Rev. B* **40**, 3616 (1989).

[28] K. Momma, F. Izumi, *J. Appl. Crystallogr.* **41**, 653 (2008).

[29] Y. Le Page, P. Saxe, *Phys. Rev. B* **65**, 104104 (2002).

[30] R. Gaillac, P. Pullumbi, F.-X. Coudert, *J. Phys. Condensed Matter* **28**, 275201 (2016).

[31] A. Marmier, Z.A.D. Lethbridge, R.I. Walton, C.W. Smith, S.C. Parker, K.E. Evans, *Comput. Phys. Commun.* **181**, 2102 (2010).

[32] A. Togo, F. Oba, I. Tanaka, *Phys. Rev. B* **78**, 134106 (2008).

[33] X. Gonze, C. Lee, *Phys. Rev. B* **55**, 10355 (1997).

[34] M. Arrigoni, G.K.H. Madsen, *Computat. Mater. Sci.* **156**, 354 (2019).

[35] L. He, F. Liu, G. Hautier, M.J.T. Oliveira, M.A.L. Marques, F.D. Vila, J.J. Rehr, G.M. Rignanese, A. Zhou, *Phys. Rev. B* **89**, 064305 (2014).

[36] P. Haas, F. Tran, P. Blaha, *Phys. Rev. B* **79**, 085104 (2009).

[37] C. Li, B. Wang, R. Wang, H. Wang, X. Lu, *Computat. Mater. Sci.* **42**, 614 (2008).

[38] W. Voigt, *Lehrbuch der Kristallphysik: mit Ausschluss der Kristalloptik*, Vol. 34, BG Teubner, Leipzig 1910.

[39] A. Reuß, *J. Appl. Math. Mech.* **9**, 49 (1929).

[40] R. Hill, *Proc. Phys. Soc. A* **65**, 349 (1952).

[41] Y. Tian, B. Xu, Z. Zhao, *Int. J. Refract. Metals Hard Mater.* **33**, 93 (2012).

[42] Ü. Bayhan, İ. Yilmaz, *Physica B Condensed Matter* **649**, 414355 (2023).

[43] Ü. Bayhan, İ. Yilmaz, "The Structural, Elastic, Electronic, Vibrational and Gravimetric Hydrogen Capacity Properties of the Perovskite Type Hydrides", *DFT Study* (2021).

[44] H. Gercek, *Int. J. Rock Mech. Mining Sci.* **44**, 1 (2007).

[45] L. Yu, Q. Yan, A. Ruzsinszky, *Nat. Commun.* **8**, 15224 (2017).

[46] Y.Ö. Çiftci, K. Çolakoğlu, E. Deligöz, Ü. Bayhan, *J. Mater. Sci. Technol.* **28**, 155 (2012).

[47] S.N. Tripathi, V. Srivastava, R. Khenata, S.P. Sanyal, *Computat. Condensed Matter* **28**, e00563 (2021).

[48] R.F.W. Bader, *Acc. Chem. Res.* **18**, 9 (1985).

[49] G. Henkelman, A. Arnaldsson, H. Jónsson, *Computat. Mater. Sci.* **36**, 354 (2006).